

ADLIFT: LIFTING ADVERSARIAL PERTURBATIONS TO SAFEGUARD 3D GAUSSIAN SPLATTING ASSETS AGAINST INSTRUCTION-DRIVEN EDITING

A PREPRINT

Ziming Hong¹ Tianyu Huang¹ Runnan Chen¹ Shanshan Ye²

Mingming Gong^{3,5} Bo Han⁴ Tongliang Liu^{1,5}

¹Sydney AI Centre, The University of Sydney ²University of Technology Sydney

³University of Melbourne ⁴Hong Kong Baptist University

⁵Mohamed bin Zayed University of Artificial Intelligence



Figure 1: (a) Unprotected 3D Gaussian Splatting (3DGS) assets are exposed to serious risks of unauthorized modification and malicious tampering. (b) In this work, we introduce AdLift, the first framework for actively safeguarding 3DGS assets, effectively preventing unauthorized manipulation across arbitrary views and editing dimensions while preserving visual fidelity. More resources are available at [project page](#).

ABSTRACT

Recent studies have extended diffusion-based instruction-driven 2D image editing pipelines to 3D Gaussian Splatting (3DGS), enabling faithful manipulation of 3DGS assets and greatly advancing 3DGS content creation. However, it also exposes these assets to serious risks of unauthorized editing and malicious tampering. Although imperceptible adversarial perturbations against diffusion models have proven effective for protecting 2D images, applying them to 3DGS encounters two major challenges: *view-generalizable protection* and *balancing invisibility with protection capability*. In this work, we propose the first editing safeguard for 3DGS, termed AdLift, which prevents instruction-driven editing across arbitrary views and dimensions by lifting strictly bounded 2D adversarial perturbations into 3D Gaussian-represented safeguard. To ensure both *adversarial perturbations effectiveness* and *invisibility*, these safeguard Gaussians are progressively optimized across training views using a tailored Lifted PGD, which first conducts *gradient truncation* during

back-propagation from the editing model at the rendered image and applies projected gradients to strictly constrain the image-level perturbation. Then, the resulting perturbation is backpropagated to the safeguard Gaussian parameters via an *image-to-Gaussian fitting* operation. We alternate between gradient truncation and image-to-Gaussian fitting, yielding consistent adversarial-based protection performance across different viewpoints and generalizes to novel views. Empirically, qualitative and quantitative results demonstrate that AdLift effectively protects against state-of-the-art instruction-driven 2D image and 3DGS editing.

1 Introduction

3D representation has become a key topic in computer vision and graphics, powering applications such as film production, game development, virtual reality, and autonomous driving. Among recent advances, 3D Gaussian Splatting (3DGS) [1] has emerged as a transformative approach that combines photorealistic fidelity with real-time rendering efficiency through an explicit Gaussian-based representation. This enables 3DGS to rapidly integrate into pipelines for creating, sharing, and deploying 3D assets across entertainment, immersive media, and autonomous systems [2, 3, 4, 5, 6, 7, 8, 9, 10], where the resulting assets naturally carry substantial value as digital content.

Recently, text-to-image latent diffusion models (LDMs) have enabled efficient and high-quality 2D image editing guided by human instructions [11]. Building upon these advances, a growing body of work have extended instruction-driven 2D editing pipelines to 3DGS [12, 13, 14]. While these methods substantially facilitate 3DGS content creation, they also expose 3DGS assets to serious risks of unauthorized modification and malicious tampering. As shown in Figure 1(a), anyone who access to 3DGS assets can perform arbitrary instruction-based editing, even without permission. *Such risks raise urgent concerns about the integrity and intellectual property of 3D assets.* Although a few prior works have explored copyright protection for 3DGS, they mainly focus on *passive protection techniques* such as 3DGS watermark and steganography [15, 16, 17, 18, 19, 20]. These passive approaches, which are only applicable for verifying asset ownership after release, are incapable of defending against instruction-driven malicious editing enabled by latent diffusion models such as InstructPix2Pix [11].

As such, this raises a natural question: *can we actively protect 3DGS assets against malicious and unauthorized editing?* Since existing 3DGS editing pipelines build upon 2D editing techniques, and several works have proposed protecting 2D images by launching *adversarial attacks* against LDMs [21, 22, 23, 24, 25, 26], it is natural to ask whether these 2D protection methods can be directly extended to 3DGS. The answer is **no**. Two key challenges arise in achieving effective protection for 3DGS:

- **View-generalizable protection:** *simultaneously suppress editing performance on the 3D representation itself as well as on 2D images rendered from arbitrary viewpoints.* A straightforward attempt for leveraging 2D image protection methods is to let a 3DGS fitting 2D views individually protected with adversarial perturbations. However, such perturbations are view-inconsistent. As illustrated in Figure 2, directly fitting may induces cross-view conflicts. Consequently, the resulting 3DGS suffers from underfitting and exhibits poor generalization to novel views.
- **Balancing invisibility with protection capability:** *preserve the appearance of the original 3DGS assets and their rendered images while retaining strong protection capability.* In 2D, unediting methods typically learn adversarial perturbations on pixel grids [27, 28], where invisibility is enforced by strict budget constraints. In contrast, 3DGS employs Gaussian primitives with a fundamentally different representation, making it nontrivial to design perturbations that are both imperceptible and effective. Existing works, which inject perturbations into Gaussian parameters (e.g., 3DGS watermarking), rely on *soft invisibility regularization* over all or selected attributes. While such soft constraints can maintain invisibility when embedding simple hidden messages into perturbations, they fail when applied to learning imperceptible adversarial perturbations against editing models. As illustrated in Figure 3, these approaches often cannot achieve a satisfactory trade-off between invisibility and adversarial attack strength.

In this work, we propose AdLift to lifting adversarial perturbations for safeguarding 3DGS assets against instruction-driven editing. Instead of relying on soft constraints or imposing hard constraints directly on Gaussian parameters, AdLift enforces strictly bounded perturbations at the 2D rendering space and then lifts them into a group of “safeguard Gaussians” in 3D space, thus achieving both attack effectiveness and invisibility. To optimize the safeguard Gaussian parameters with hard constraint on rendering space, we introduce a tailored Lifted PGD (L-PGD), which contains two steps: (i) *gradient truncation* to enforce strict invisibility constraints, and (ii) *image-to-Gaussian fitting* to update the 3D parameters accordingly. Specifically, L-PGD truncate the gradient during back-propagation from the editing model to the Gaussians at the rendered image and apply projected gradients to strictly constrain the image-level perturbation. Then, the perturbation is backpropagated to the Gaussian parameters via an image-to-Gaussian fitting operation. L-PGD alternates between *gradient truncation* and *image-to-Gaussian fitting*, progressively seeking the optimal Gaussian-represented adversarial perturbations with both consistent attack performance and invisibility across

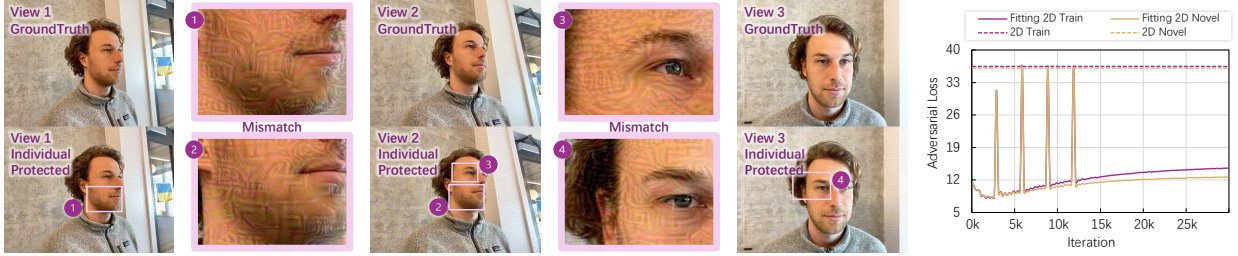


Figure 2: (Left): mismatching between view-specific adversarial perturbations¹ learned individually on different views of a face scene. (Right): multi-view inconsistencies cause underfitting, resulting in a large adversarial loss gap compared with 2D-trained perturbations (denoted as 2D Train/Novel).



Figure 3: Perturbations¹ imposed on spherical-harmonic (SH) features (i.e., GuardSplat [16]) under soft invisibility constraints (e.g., SSIM) pose inherent challenges in balancing invisibility and attack strength. (Left): Perturbations learned by GuardSplat. (Right): PSNR-Adversarial Loss scatter plot over multiple runs under different attack-invisibility trade-off weights.

different viewpoints, thus yielding view-consistent adversarial-based unediting safeguards that generalize effectively to novel views.

Empirically, we validate the protection performance of AdLift against instruction-driven 2D image editing and instruction-driven global/local 3DGS editings on two forward-face scenes and two 360degree scenes. Extensive experiments demonstrate the state-of-the-art protection performance of AdLift. *Typically examples are shown in Figure 1(b).* Our main contributions are three-fold:

- We investigate the problem of active copyright protection for 3D Gaussian Splatting assets against instruction-driven editing. In particular, we identify two key challenges: (i) *view-generalizable protection*, and (ii) *balancing invisibility with protection capability*.
- We propose the first framework, AdLift, which protects 3DGS assets against instruction-driven unauthorized editing. Specifically, AdLift trains a group of dedicated safeguard Gaussians using a tailored Lifted PGD (L-PGD), which lifts strictly bounded perturbations from the 2D image space into the 3D Gaussian space to ensure both invisibility and attack effectiveness.
- Extensive experiments on four 3DGS scenes and diverse instruction-driven editing tasks (2D/3D, global/local) demonstrate the general effectiveness of our AdLift.

2 Related Work

Copyright protection for 3DGS. Recent efforts have extended copyright protection techniques to 3DGS, including watermarking [15, 16, 29, 30, 31, 17] and steganography [18, 19, 20]. These approaches hide information within 3DGS assets by introducing imperceptible perturbations, serving as ownership watermarks or as steganographic payloads, that can be reliably extracted from both the 3D representation and its rendered 2D images. To preserve visual fidelity, their perturbations are typically restricted to specific Gaussians or their attributes. For example, Gaussian-Marker [15] densifies high-uncertainty regions by adding new Gaussians whose parameters are optimized to carry watermark signals, while GuardSplat [16] perturbs only the spherical-harmonic (SH) features of existing Gaussians to embed watermarks without altering geometry. In both cases, watermark decoding objectives are jointly optimized with soft fidelity regularization (e.g., SSIM) to mitigate artifacts and maintain rendering quality. However, existing watermarking- or steganography-based methods provide only *passive copyright protection for 3DGS assets*, e.g., *they only enable ownership verification* [32] by extracting identity messages from potentially leaked assets. Such passive schemes, however, are incapable of actively defend [33, 34, 35, 36, 37, 38, 39] against malicious editing (e.g., forgery or tampering) enabled by recent instruction-driven 2D image and 3DGS editing techniques [11, 40, 12].

¹We here conduct an untargeted attack in Equation (8); higher loss means a stronger attack strength.

Edit Guard for 2D Image. Recent studies have investigated protection for 2D images against unauthorized editing and tampering [41, 26, 23, 42, 43, 24, 22, 44, 25, 21]. The core idea is to formulate protection as an adversarial attack [27, 28, 45, 46, 47, 48, 49] on editing models, injecting imperceptible perturbations into images so that downstream editing fails or produces extremely degraded qualities. However, despite the success of 2D image guards, their extension to 3DGS remains unexplored and introduces unique challenges, including the need to enforce *view-consistent perturbations for view-generalizable protection* and to *balance invisibility against protection effectiveness*.

3 Preliminary

3D Gaussian Splatting (3DGS). 3DGS [1] is an efficient explicit 3D representation that models a scene using anisotropic Gaussians, where each Gaussian G is defined by mean $\mu \in \mathbb{R}^3$, covariance matrix Σ (factorized as $\Sigma = RSS^\top R^\top$, with scaling $S \in \mathbb{R}^3$ and rotation $R \in \mathbb{R}^{3 \times 3}$), color $c \in \mathbb{R}^3$, and opacity $\alpha \in \mathbb{R}$. A Gaussian centered at μ can be expressed as: $G(p) = \exp(-\frac{1}{2}(p - \mu)^\top \Sigma^{-1}(p - \mu))$, where p denotes any 3D position. When rendering, the 3D Gaussians are projected into 2D and composited along each camera ray using a volume splatting method. Specifically, the color C of a pixel is computed by blending N depth-ordered points: $C = \sum_{i \in \mathcal{N}} c_i \alpha_i \prod_{j=1}^{i-1} (1 - \alpha_j)$, where c_i is the color estimated by the spherical harmonics (SH) coefficients of each Gaussian, and α_i is given by evaluating a 2D Gaussian with covariance Σ' [50] multiplied with a per-point opacity. By integrating all Gaussians G , the 3DGS model \mathcal{G} forms a compact yet expressive representation of complete 3D scenes.

Instruction-driven Image Editing. Latent Diffusion Models (LDMs) [51] serve as the backbone for modern image editing. In LDM, an Variational Autoencoder (VAE), consisting of an encoder \mathcal{E} and a decoder \mathcal{D} , first maps an image x into a latent code $z = \mathcal{E}(x)$. In the latent space, a diffusion model ϵ_θ then learns to denoise the noised latent z_t at each time step t , conditioned on an embedding $c_\theta(y)$ derived from the input y . The standard LDM training objective is: $\mathcal{L}_{\text{LDM}} = \mathbb{E}_{z, y, \epsilon, t} [\|\epsilon - \epsilon_\theta(z_t, t, c_\theta(y))\|_2^2]$, where z_t is the latent corrupted to step t , ϵ is the Gaussian noise sample. Furthermore, **InstructPix2Pix (IP2P)** [11] extends LDMs to directly follow human editing instructions. IP2P fine-tunes the LDM on triplets $(x^{\text{src}}, y, x^{\text{edit}})$, where x^{src} is the source image, y is the instruction, and x^{edit} is the corresponding edited image. The training objective is: $\mathcal{L}_{\text{IP2P}} = \mathbb{E}_{z^{\text{edit}}, z_0, y, \epsilon, t} [\|\epsilon - \epsilon_\theta(z_t^{\text{edit}}, t, z_0, c_\theta(y))\|_2^2]$, where $z_0 = \mathcal{E}(x^{\text{src}})$ is the latent codes of source image, z_t^{edit} is the noisy latent of the target image at step t . The denoiser ϵ_θ is conditioned jointly on the original image latent z_0 and the instruction embedding $c_\theta(y)$. Through this fine-tuning, IP2P *enables users to perform direct, instruction-driven edits on input images, yielding results that faithfully follow human-provided instructions*.

Instruction-guided 3DGS editing. Given a source 3DGS model \mathcal{G}^{src} and a user-specified editing instruction y , the objective of instruction-guided 3DGS editing is to transform \mathcal{G}^{src} into an edited version $\mathcal{G}^{\text{edit}}$ that complies with y . Current approaches achieve this by leveraging 2D image editing techniques [14, 52, 12, 53, 13, 54, 55, 40]. Specifically, \mathcal{G}^{src} is first rendered from multiple training views $\mathcal{V}^t = \{v_i^t\}_{i=1}^{N_t}$ to produce a set of source images $\mathcal{I}^{\text{src}} = \{x_i^t = \mathcal{R}(\mathcal{G}, v_i^t)\}_{i=1}^{N_t}$. A 2D editing model (e.g., IP2P) then modifies \mathcal{I}^{src} into edited images $\mathcal{I}^{\text{edit}}$ according to the specified instruction y . These edited images provide supervision for updating \mathcal{G}^{src} , yielding the edited $\mathcal{G}^{\text{edit}}$ by minimizing the editing loss $\mathcal{L}_{\text{Edit}}$ across all training views \mathcal{V} :

$$\mathcal{G}^{\text{edit}} = \arg \min_{\mathcal{G}} \sum_{v^t \in \mathcal{V}} \mathcal{L}_{\text{Edit}}(\mathcal{R}(\mathcal{G}, v^t), \mathcal{I}^{\text{edit}}), \quad (1)$$

where \mathcal{R} denotes the rendering function that projects a 3DGS into an image under view v . Besides, multi-view consistency constraints can be introduced to Equation (1) for preventing mode collapse and low-quality results caused by inconsistencies in the 2D guidance images [12].

4 AdLift: Lifting Adversarial Perturbations on 3DGS

4.1 Problem Statement

Assumptions on asset owner’s capability. We assume the defender has *white-box* access to one or more instruction-guided editing models used to simulate attacks during protection design, but *no control over the editing instructions provided by potential attackers*. This assumption enables us to clearly formulate the protection task and to demonstrate the feasibility of adversarially optimized defenses in the 3DGS domain. Furthermore, we assume the defender has access to the original 3DGS asset \mathcal{G}^{raw} trained on multi-view ground-truth images $\mathcal{I}^t = \{x_v^t | v \in \mathcal{V}^t\}$, where $\mathcal{V}^t = \{v_i^t\}_{i=1}^{N_t}$.

Protection objective. Our objective is to design a protection mechanism for transform \mathcal{G}^{raw} into $\mathcal{G}^{\text{prot}}$ through slight modifications that **preserve visual fidelity** while enforcing the following properties:

- **2D protection:** Any rendered view from $\mathcal{G}^{\text{prot}}$ remains robust against instruction-guided 2D image editing methods, thereby preventing attackers from exploiting view-wise manipulations.
- **3D protection:** The entire asset $\mathcal{G}^{\text{prot}}$ cannot be effectively manipulated by instruction-guided 3DGS editing methods, ensuring the integrity and semantic consistency of the original 3D content.

4.2 Rethinking Gaussians-represented Perturbations

This task can be regarded as a natural extension of *edit guards* in the 2D image domain, which typically construct *adversarial perturbations* [27, 28, 21] to prevent image editing by instruction-tuned diffusion models. Specifically, for a single 2D image x^t , the protected image x^{prot} can be derived via optimize the following objective:

$$x^{\text{prot}} = \arg \min_x \mathcal{L}_{\text{adv}}(x, y) \quad \text{s.t. } \|x - x^t\|_{\infty} \leq \eta, \quad (2)$$

where $\mathcal{L}_{\text{adv}}(\cdot, y)$ is the adversarial loss² enforcing resistance against the editing model under instruction y , $\|\cdot\|_{\infty}$ represents the ∞ -norm which measures perturbation magnitude, and η controls the perturbation budget to ensure imperceptibility. Intuitively, the objective seeks a perturbed x^{prot} that remains visually indistinguishable from x while disrupting the effect of instruction-guided editing.

However, directly extending 2D defenses to 3DGS leaves a critical gap. A straightforward attempt is to fitting the protected model $\mathcal{G}^{\text{prot}}$ on multiple 2D protected training views $\{x_{v^t}^{\text{prot}}\}, v^t \in \mathcal{V}^t$:

$$\mathcal{G}^{\text{prot}} = \arg \min_{\mathcal{G}} \sum_{v^t \in \mathcal{V}^t} \mathcal{L}_{\text{rec}}(\mathcal{R}(\mathcal{G}, v^t), x_{v^t}^{\text{prot}}), \quad (3)$$

where $\mathcal{R}(\mathcal{G}, v^t)$ is its rendering under view v^t , and \mathcal{L}_{rec} is a photometric reconstruction loss (like SSIM). Unfortunately, independently optimized perturbations on are not view-consistent, leading to *cross-view conflicts*, as illustrated in Figure 2. As a result, training $\mathcal{G}^{\text{prot}}$ causes underfitting even on training views and severely degrades generalization to unseen viewpoints.

Considering the natively view-continuity of Gaussians, several works [15, 16] use a group of Gaussians to represent perturbations and train them from the 3D space or dynamically from 2D views, rather than directly fitting in-consistent 2D supervisions. However, unlike the directly fitting where objectives $\{x_{v^t}^{\text{prot}}\}$ already satisfy both the imperceptible and protection requirements, *a critical challenge for training Gaussian-represented perturbation is how to preserve the appearance consistency between $\mathcal{G}^{\text{prot}}$ and \mathcal{G}^{raw} while retaining strong protection capability*.

Gaussians-represented perturbations are not easy to set a suitable perturbation bound. In Equation (2), unediting methods for 2D images typically learn adversarial perturbations on pixel grids, with invisibility enforced by predefined budget η constraints and projection operations [28]. In contrast, 3DGS employs Gaussian primitives with a fundamentally different representation, making it nontrivial to design invisible yet effective perturbations³. Existing works which try to learn Gaussian-represented perturbations [15, 16] typically add **soft constraints** via invisible regularization on all or selected Gaussian attributes for maintaining perturbation imperceptibility. Although being effective for hidden messages in perturbations, these approaches fail to strike a satisfactory balance between imperceptibility and adversarial attack strength for instruction-based editing models, as illustrated in Figure 3.

4.3 Rendering-space Strictly Bound for Gaussians-represented Perturbations

In order to balance imperceptibility and protection strength of 3DGS perturbations, we propose to impose **strictly bounded constraints** on rendering view space. Formally, the objective of learning 3DGS adversarial perturbations can be formulated as:

$$\mathcal{G}^{\text{prot}} = \arg \min_{\mathcal{G}} \sum_{v^t \in \mathcal{V}^t} \mathcal{L}_{\text{adv}}(\mathcal{R}(\mathcal{G}, v^t), y) \quad \text{s.t. } \|\mathcal{R}(\mathcal{G}, v^t) - \mathcal{R}(\mathcal{G}^{\text{raw}}, v^t)\|_{\infty} \leq \eta, \quad \forall v^t \in \mathcal{V}^t, \quad (4)$$

where we set a strictly upper bound η (i.e., the perturbation budget) via the ∞ -norm on all the training views. Intuitively, by enforcing perturbation bounds in the image domain, our approach circumvents the instability of soft regularizations and the difficulty of hard Gaussian-parameter constraints, thus ensuring perceptually meaningful control and consistent invisibility across views.

²Without loss of generality, we assume smaller \mathcal{L}_{adv} indicates better attack performance.

³Heterogeneous attributes (e.g., position, scale, color, opacity) make uniform budgets ineffective.

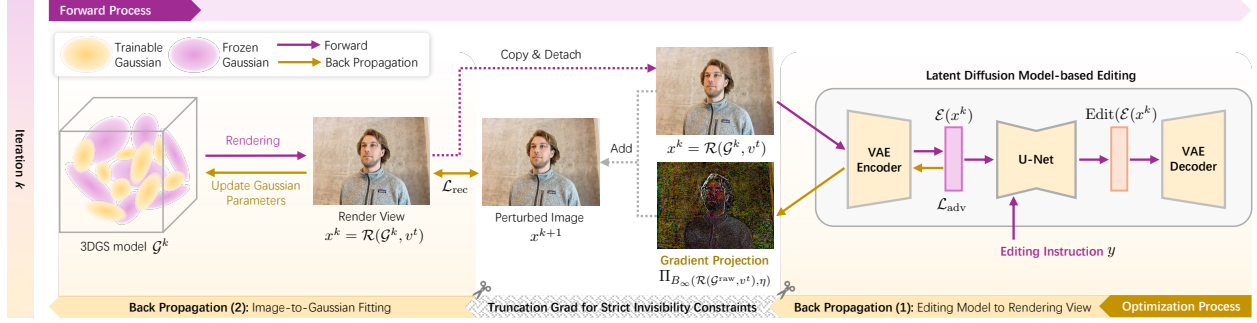


Figure 4: The proposed method AdLift, where a tailored Lifted PGD (L-PGD) is used for learning Gaussians-represented adversarial perturbations against Instruction-based editing models. L-PGD alternates between *gradient truncation*, which enforces invisibility in the image domain, and *image-to-Gaussian fitting*, which propagates the constrained perturbations back into the 3D space.

4.4 Lifted Projected Gradient Descent

Solving the optimization problem in Equation (4) is not straightforward. Considering the k -th iteration and for a given training view v^t , the update rule of gradient descent-based solver for Equation (4) can be formulated as:

$$G^{k+1} = \Pi_C(G^k - \alpha \cdot \nabla_G \mathcal{L}_{\text{adv}}(\mathcal{R}(G^k, v^t), y)), \quad (5)$$

where Π_C denotes projection onto the feasible set $\mathcal{C} = \{G : \|\mathcal{R}(G, v^t) - \mathcal{R}(G^{\text{src}}, v^t)\|_{\infty} \leq \eta, \forall v^t \in \mathcal{V}^t\}$. Equation (5) requires (i) *updating Gaussian parameters in the 3D space to minimize the adversarial loss*, while (ii) *enforcing hard constraints in the image domain across multiple rendered views to ensure visual quality*. The discrepancy between the optimization variables (3D Gaussian primitives) and the constraint space (multi-view 2D projections) complicates the problem.

To solve Equation (4), we introduce a tailored Lifted PGD (L-PGD). As shown in Figure 4, L-PGD consists of two main steps: (i) *gradient truncation to enforce strict invisibility constraints*, and (ii) *image-to-Gaussian fitting to update the 3D parameters accordingly*.

Gradient truncation for strict invisibility constraints. Although feasible set \mathcal{C} is *implicitly* defined in the 3D Gaussian parameter space, its explicit characterization becomes available in the rendered image space. This means that while we may not know the precise form of \mathcal{C} in Gaussian-parameter space, we can still approximate it by evaluating surrogate renderings from the prospective update of G that achieves a smaller adversarial loss. Let $x^k = \mathcal{R}(G^k, v^t)$ denote the current rendered image, we truncate the gradient in Equation (5) on the image domain, so the projected update becomes:

$$x^{k+1} = \Pi_{B_{\infty}(\mathcal{R}(G^{\text{raw}}, v^t), \eta)} [x^k - \alpha \cdot \text{sign}(\nabla_x \mathcal{L}_{\text{adv}}(x^k, y))], \quad (6)$$

where $B_{\infty}(x, \eta)$ denotes the ℓ_{∞} ball of radius η centered at $\mathcal{R}(G^{\text{raw}}, v^t)$. This guarantees that the updated rendering x^{k+1} strictly satisfies the hard imperceptibility constraint, i.e., it can be regarded as the rendered image of a hypothetical $(k+1)$ -th 3DGS model \hat{G}^{k+1} , with $\mathcal{R}(\hat{G}^{k+1}, v^t) = x^{k+1}$, where \hat{G}^{k+1} necessarily lies within the feasible set \mathcal{C} and has smaller adversarial loss.

Image-to-Gaussian fitting. Given the current 3DGS model G^k and the surrogate rendered image $x^{k+1} = \mathcal{R}(\hat{G}^{k+1}, v^t)$ from a hypothetical next-step Gaussian model \hat{G}^{k+1} that achieves a smaller adversarial loss, we treat x^{k+1} as a supervision signal. The Gaussian parameters of G^k are then updated by fitting its rendering $\mathcal{R}(G^k, v^t)$ to x^{k+1} . Formally, given the training view v^t , the update rule of the image-to-Gaussian fitting step can be formulated as:

$$G^{k+1} = G^k - \beta \cdot \nabla_G \mathcal{L}_{\text{rec}}(\mathcal{R}(G^k, v^t), x^{k+1}), \quad (7)$$

where β is the learning rate for the image-to-Gaussian fitting step and \mathcal{L}_{rec} is a reconstruction loss. In this way, G^{k+1} is optimized toward the hypothetical next-step Gaussians, thereby remaining within the feasible set while achieving a smaller adversarial loss.

Alternating optimization. The safeguard Gaussians G^{prot} are jointly and progressively optimized across all training views $v^t \in \mathcal{V}^t$. L-PGD alternates between *gradient truncation*, which enforces invisibility in the image domain, and *image-to-Gaussian fitting*, which propagates the constrained perturbations back into the 3D space. Through this alternating process, G^{prot} is optimized to minimize the adversarial loss while simultaneously satisfying strict imperceptibility bounds across multiple viewpoints. The overall algorithm for training AdLift via L-PGD is shown in Algorithm 1.

Intuitively, L-PGD optimizes safeguard Gaussians $\mathcal{G}^{\text{prot}}$ by lifting strictly bounded and multi-view consistent adversarial perturbations from the 2D rendered image domain into the intrinsic 3D Gaussian space. The dynamic alternating optimization procedure in L-PGD avoids the need to manually assign heterogeneous budgets on Gaussian parameters, which are difficult to calibrate and may cause visible distortions if mis-specified. Instead, the *rendering-space bound* ensures that every intermediate update is constrained to remain visually indistinguishable from the original views, while the *image-to-Gaussian fitting* propagates these perturbations back into 3D Gaussian parameters. In this way, the safeguard Gaussians inherit the adversarial protection strength observed in individual 2D cases, but extend it coherently across all viewpoints, thereby ensuring continuous and cross-view consistent protection.

Algorithm 1 Training AdLift via Lifted PGD (L-PGD).

```

1: Input: Training views  $\mathcal{V}^t$ ; unprotected model  $\mathcal{G}^{\text{raw}}$  and trainable model with safeguard  $\mathcal{G}$ ; Total iterations  $E$ ; Gradient truncation iterations  $K_p$ ; Image-to-Gaussian fitting iterations  $K_l$ ; Learning rates  $\alpha, \beta$ ; Perturbation budget  $\eta$ .
2: for  $k = 1$  to  $E - 1$  do
3:   Sample a training view  $v^t \sim \mathcal{V}^t$ ;
4:   Render:  $x^{k(1)} = \mathcal{R}(\mathcal{G}^k, v^t)$ ,  $x = \mathcal{R}(\mathcal{G}^{\text{raw}}, v^t)$ ;
5:   for  $i = 1$  to  $K_p - 1$  do
6:      $x^{k(i+1)} = \Pi_{B_\infty(x, \eta)}[x^{k(i)} - \alpha \text{sign}(\nabla_x \mathcal{L}_{\text{adv}}(x^{k(i)}))]$ ;
7:   end for
8:   Let  $x^{k+1} = x^{k(K_p)}$ , and  $\mathcal{G}^{k(1)} = \mathcal{G}^k$ ;
9:   for  $j = 1$  to  $K_l - 1$  do
10:     $\mathcal{G}^{k(j+1)} = \mathcal{G}^{k(j)} - \beta \nabla_{\mathcal{G}} \mathcal{L}_{\text{rec}}(\mathcal{R}(\mathcal{G}^{k(j)}, v^t), x^{k+1})$ ;
11:   end for
12:   Let  $\mathcal{G}^{k+1} = \mathcal{G}^{k(K_l)}$ ;
13: end for
14: Output: Trained safeguard Gaussians  $\mathcal{G}^{\text{prot}} = \mathcal{G}^E$ .

```

4.5 Adversarial Objectives for Resisting Editing Model

L-PGD is compatible with various adversarial loss functions \mathcal{L}_{adv} , enabling the design of different AdLift variants tailored to specific requirements. We illustrate several representative cases of adversarial attacks on instruction-based 2D and 3D global/local editing tasks. As directly attacking the diffusion model itself has proven challenging [56, 57], we instead target other *instruction-agnostic* components integrated in instruction-driven editing pipelines:

- *Attack VAE (Untargeted)*: Encourage the latent code of the rendered image $\mathcal{R}(\mathcal{G}, v^t)$ to deviate from that of the raw rendering, which breaks the original representation and leads to artifacts that hinder faithful instruction-driven editing:

$$\mathcal{L}_{\text{VU}} = -\|\mathcal{E}(\mathcal{R}(\mathcal{G}, v^t)) - \mathcal{E}(\mathcal{R}(\mathcal{G}^{\text{raw}}, v^t))\|_2^2. \quad (8)$$

- *Attack VAE (Targeted)*: Also referred to as *Textural Loss* [24, 42, 23, 22]. This loss aligns the latent code of $\mathcal{R}(\mathcal{G}, v^t)$ with that of a chosen target image or pattern x^{target} , injecting irrelevant textures that compromise realism and misguide the editing process:

$$\mathcal{L}_{\text{VT}} = \|\mathcal{E}(\mathcal{R}(\mathcal{G}, v^t)) - \mathcal{E}(x^{\text{target}})\|_2^2. \quad (9)$$

- *Attack Segment-Anything (SAM)*: Given a rendered image $\mathcal{R}(\mathcal{G}, v^t)$, SAM [58] $\mathcal{S}(\mathcal{R}(\mathcal{G}, v^t), b)$ predicts a mask conditioned on bounding box b , which is widely adopted in 3DGS editing for local region localization. Thus, we enforce the predicted mask to match a target mask m^{target} for misguiding segmentation, resulting in unnatural boundaries and corrupted local edits:

$$\mathcal{L}_{\text{ST}} = \mathcal{L}_{\text{BCE}}(\mathcal{S}(\mathcal{R}(\mathcal{G}, v^t), b), m^{\text{target}}) + \lambda_{\text{Dice}} \mathcal{L}_{\text{Dice}}(\mathcal{S}(\mathcal{R}(\mathcal{G}, v^t), b), m^{\text{target}}), \quad (10)$$

where m^{target} is the desired mask and λ_{Dice} controls the relative weight of the two terms.

5 Experiments

Datasets: We collect two forward-facing scenes from [59] and [60] and two 360degree scenes from [59] and [61]. **Edit baselines:** For *Instruction-based Image Editing*, we use IP2P [11], and for *Instruction-based 3DGS Editing*, we choose instruction-based editing methods: Instruct-GS2GS [40, 59] and DGE [12]. **Protect baselines:** We compare (i): asset without protection, (ii) soft constraints in GuardSplat [16], and (iii) fitting the 3DGS on 2D protected images (i.e., Equation (3), denoted as Fit2D). **Evaluation metrics:** *Invisibility*: We evaluate the visual similarity of views rendered from the models and ground truth using SSIM [62], PSNR, and LPIPS [63]. *Protection Capability*: We use two metrics for measuring protection effectiveness: CLIP Text-Image Directional Similarity (CLIP_d) and CLIP Image Similarity (CLIP_s). **Implementation for AdLift**: We have two ways for initialization: (i) copy all of the original gaussians for the unprotected asset \mathcal{G}^{raw} , and use these new gaussians as trainable parameters while fix all of the original Gaussians. We denote this as AdLift. (ii) we can also continue training our AdLift on the 3DGS which directly fitting on independent 2D adversarial perturbations. We denote it as AdLift*. Beside, we mark different adversarial objectives after the method name⁴. **Implementation for editing**: We use default hyper-parameters for each editing method. Editing instructions are parts collected from previous works [52] and further extended by using GPT-5 and humanly reviewed. The complete editing instructions are shown in Appendix H.2. We conduct each

⁴For example, AdLift-VU means training AdLift by using the untargeted VAE loss in Equation (8).

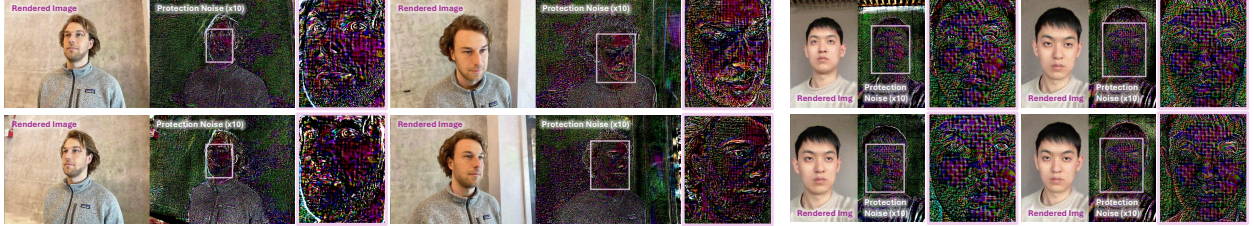
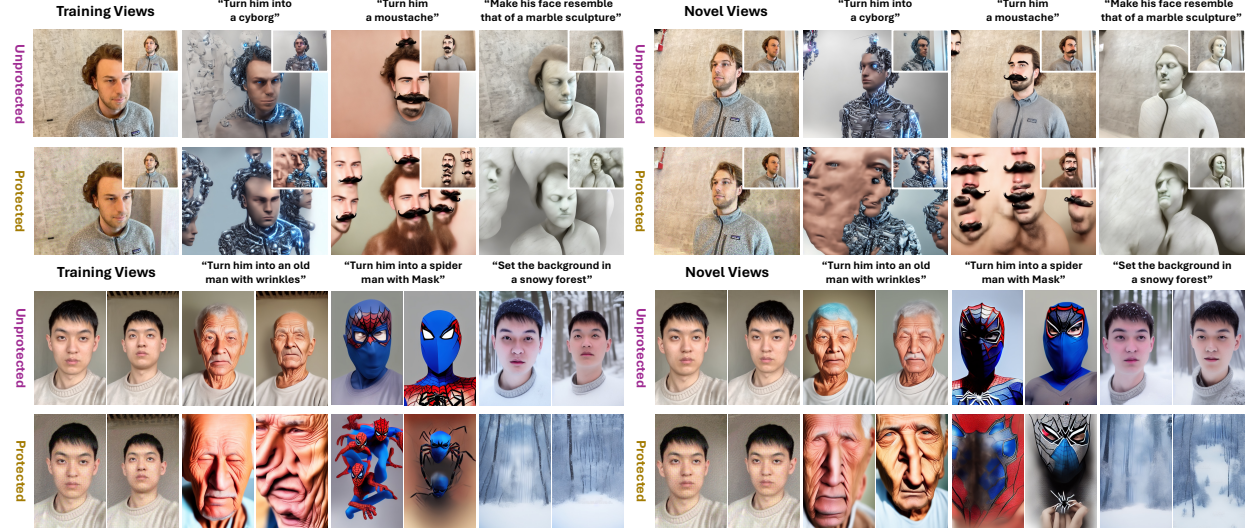


Figure 5: Visualization of protection perturbations learned by AdLift*-VU.

Figure 6: Qualitative results of *instruction-based image editing* on two face scenes. We show the comparison of editing results of unprotected 3D assets and 3D assets protected by AdLift*-VU.Table 1: Results of *instruction-based image editing* (averaged across four scenes). We report results on both *training* and *novel views*. The best/second best results are denoted as **bold**/underline.

Method	Training Views				Novel Views					
	Invisibility		Protection Quality		Invisibility		Protection Quality			
	SSIM(\uparrow)	PSNR(\uparrow)	LPIPS(\downarrow)	CLIP _d (\downarrow)	CLIP _s (\downarrow)	SSIM(\uparrow)	PSNR(\uparrow)	LPIPS(\downarrow)	CLIP _d (\downarrow)	CLIP _s (\downarrow)
No Protection	0.9215	30.4812	0.0805	0.1875	0.8892	0.8061	25.0546	0.1322	0.1901	0.8819
Fit2D-VU	0.7557	27.0716	0.2566	0.1797	0.8368	0.6478	23.7012	0.2882	0.1825	0.8488
Fit2D-VT	0.8232	<u>27.9244</u>	<u>0.1433</u>	0.1752	0.8566	0.7168	24.3197	<u>0.1869</u>	0.1798	0.8592
AdLift-VU	0.7751	27.7292	0.2528	0.1787	0.8139	0.6802	23.7918	0.2841	0.1799	0.8181
AdLift-VT	<u>0.8133</u>	<u>27.8060</u>	<u>0.1670</u>	0.1748	0.8370	0.7182	23.8981	<u>0.2095</u>	<u>0.1782</u>	0.8366
AdLift*-VU	0.7280	27.4019	0.3069	0.1806	0.7889	0.6374	23.9092	0.3330	0.1802	0.8087
AdLift*-VT	0.7896	27.6083	0.1848	0.1731	0.8258	0.7008	<u>24.0815</u>	0.2240	0.1758	0.8296

instruction for three times, and get the average results. All experiments are conducted on NVIDIA RTX 4090 GPU. More details are shown in Appendix H.

5.1 Evaluation on Instruction-based Image Editing

We show **visualization of protection perturbations** in Figure 5, the adversarial noise (amplified $\times 10$ for visualization) learned by AdLift remains spatially coherent across different viewpoints. In particular, semantic regions such as the face and hair are perturbed in a consistent manner rather than producing mismatched or fragmented patterns. **Qualitative results** for protection are shown in Figure 6. We present comparisons of instruction-driven editing applied to both unprotected and AdLift-protected 3DGS assets. Compared to unprotected, assets protected by AdLift effectively resist editing either on training views and novel views, producing unrealistic editing results by following the instructions. Importantly, this protection generalizes from training to novel views, demonstrating that our lifted perturbations enforce view-consistent and generalizable safeguards. Besides, we present **quantitative results** in Table 1. From the results, our AdLift consistently achieves stronger protection (lower CLIP_d and CLIP_s) while maintaining competitive invisibility metrics (SSIM, PSNR, LPIPS) across both training and novel views. These results demonstrate that our lifted perturbations provide an effective balance between imperceptibility and protection quality.



Figure 7: Instruction-based global 3DGS editing for assets w/o and w/ AdLift*-VU protection.



Figure 8: Instruction-based local 3DGS editing for unprotected and AdLift*-ST protected assets.

5.2 Instruction-based 3DGS Editing Results

Figures 7, 8 present **qualitative results** on instruction-driven 3DGS global editing (Instruct-GS2GS [40]) and local editing (DGE [12]). For global editing, our AdLift, similar to the 2D case, effectively disrupts editing on 3DGS assets, preventing the intended transformations. For local editing, the SAM-based loss misguides region localization, thereby preserving the original appearance of the assets by rendering them resistant to instruction-based edits. **Quantitatively**, as shown in Table 2, our approach achieves consistently lower $CLIP_d$ and $CLIP_s$ scores across both training and novel views, confirming superior protection quality over unprotected assets.

More results are shown in Appendices, including but not limited to: Appendix A: Comparing training dynamic for Fit2D, and different variants of AdLift; Appendix B: Comparison with soft constraint methods for learning 3DGS perturbations; Appendix C: More qualitative and quantitative results of AdLift; Appendix D: Robustness to editing hyperparameters; Appendix E: Analysis of AdLift hyperparameters; Appendix F: Analysis of transferability, robustness, and generality of AdLift; Appendix G: More discussion and limitation for this work; and Appendix H: More experimental details and the full editing instructions.

6 Conclusion

In this work, we explore anti-editing protection in the context of 3D Gaussian Splatting. For *achieving view-generalizable protection and maintaining a delicate balance between invisibility and protection strength*, we introduce AdLift, a novel framework that trains safeguard Gaussians via a tailored Lifted PGD strategy, lifting bounded perturbations from the 2D image domain into the 3D Gaussian space. Extensive experiments on multiple 3DGS scenes and a wide range of editing tasks demonstrate that AdLift provides view-consistent and imperceptible protection, marking a significant step toward securing 3D assets against unauthorized instruction-driven editing.

Table 2: Quantitative evaluations on instruction-based 3DGS editing.

Method	Training Views		Novel Views	
	$CLIP_d(\downarrow)$	$CLIP_s(\downarrow)$	$CLIP_d(\downarrow)$	$CLIP_s(\downarrow)$
Instruct-GS2GS				
No Protection	0.1372	—	0.1251	—
AdLift*-VT	0.1321	0.8665	0.1166	0.8693
AdLift*-VU	0.1373	0.8276	0.1180	0.8321
DGE (Global)				
No Protection	0.1287	—	0.1296	—
AdLift*-VT	0.1146	0.9219	0.1162	0.9229
AdLift*-VU	0.1156	0.9024	0.1176	0.9037
DGE (Local)				
No Protection	0.1337	—	0.1321	—
AdLift*-ST	0.0389	0.8593	0.0425	0.8618

References

- [1] Bernhard Kerbl, Georgios Kopanas, Thomas Leimkühler, and George Drettakis. 3d gaussian splatting for real-time radiance field rendering. *ACM Trans. Graph.*, 42(4):139–1, 2023.
- [2] Runnan Chen, Xiangyu Sun, Zhaoqing Wang, Youquan Liu, Jiepeng Wang, Lingdong Kong, Jiankang Deng, Mingming Gong, Liang Pan, Wenping Wang, et al. Ovgaussian: Generalizable 3d gaussian segmentation with open vocabularies. *arXiv preprint arXiv:2501.00326*, 2024.
- [3] Youquan Liu, Lingdong Kong, Weidong Yang, Xin Li, Ao Liang, Runnan Chen, Ben Fei, and Tongliang Liu. La la lidar: Large-scale layout generation from lidar data. *arXiv preprint arXiv:2508.03691*, 2025.
- [4] Haodong Chen, Runnan Chen, Qiang Qu, Zhaoqing Wang, Tongliang Liu, Xiaoming Chen, and Yuk Ying Chung. Beyond gaussians: Fast and high-fidelity 3d splatting with linear kernels. *arXiv preprint arXiv:2411.12440*, 2024.
- [5] Runnan Chen, Youquan Liu, Lingdong Kong, Xinge Zhu, Yuexin Ma, Yikang Li, Yuenan Hou, Yu Qiao, and Wenping Wang. Clip2scene: Towards label-efficient 3d scene understanding by clip. In *Proceedings of the IEEE/CVF Conference on Computer Vision and Pattern Recognition (CVPR)*, pages 7020–7030, June 2023.
- [6] Xiangyu Sun, Runnan Chen, Mingming Gong, Dong Xu, and Tongliang Liu. Intern-gs: Vision model guided sparse-view 3d gaussian splatting. *arXiv preprint arXiv:2505.20729*, 2025.
- [7] Jiaxin Huang, Ziwen Li, Hanlve Zhang, Runnan Chen, Xiao He, Yandong Guo, Wenping Wang, Tongliang Liu, and Mingming Gong. Surprise3d: A dataset for spatial understanding and reasoning in complex 3d scenes. *arXiv preprint arXiv:2507.07781*, 2025.
- [8] Jiaxin Huang, Runnan Chen, Ziwen Li, Zhengqing Gao, Xiao He, Yandong Guo, Mingming Gong, and Tongliang Liu. Mllm-for3d: Adapting multimodal large language model for 3d reasoning segmentation. *arXiv preprint arXiv:2503.18135*, 2025.
- [9] Ziwen Li, Jiaxin Huang, Runnan Chen, Yunlong Che, Yandong Guo, Tongliang Liu, Fakhri Karray, and Mingming Gong. Urbangs: Semantic-guided gaussian splatting for urban scene reconstruction. *arXiv preprint arXiv:2412.03473*, 2024.
- [10] Zhuo Huang, Chang Liu, Yinpeng Dong, Hang Su, Shibao Zheng, and Tongliang Liu. Machine vision therapy: Multimodal large language models can enhance visual robustness via denoising in-context learning. In *Forty-first International Conference on Machine Learning*, 2024.
- [11] Tim Brooks, Aleksander Holynski, and Alexei A Efros. Instructpix2pix: Learning to follow image editing instructions. In *Proceedings of the IEEE/CVF conference on computer vision and pattern recognition*, pages 18392–18402, 2023.
- [12] Minghao Chen, Iro Laina, and Andrea Vedaldi. Dge: Direct gaussian 3d editing by consistent multi-view editing. In *European Conference on Computer Vision*, pages 74–92. Springer, 2024.
- [13] Yiwen Chen, Zilong Chen, Chi Zhang, Feng Wang, Xiaofeng Yang, Yikai Wang, Zhongang Cai, Lei Yang, Huaping Liu, and Guosheng Lin. Gaussianeditor: Swift and controllable 3d editing with gaussian splatting. In *Proceedings of the IEEE/CVF conference on computer vision and pattern recognition*, pages 21476–21485, 2024.
- [14] Dong In Lee, Hyeongcheol Park, Jiyoung Seo, Eunbyung Park, Hyunje Park, Ha Dam Baek, Sangheon Shin, Sangmin Kim, and Sangpil Kim. Editsplat: Multi-view fusion and attention-guided optimization for view-consistent 3d scene editing with 3d gaussian splatting. In *Proceedings of the Computer Vision and Pattern Recognition Conference*, pages 11135–11145, 2025.
- [15] Xiufeng Huang, Ruiqi Li, Yiu-ming Cheung, Ka Chun Cheung, Simon See, and Renjie Wan. Gaussianmarker: Uncertainty-aware copyright protection of 3d gaussian splatting. *Advances in Neural Information Processing Systems*, 37:33037–33060, 2024.
- [16] Zixuan Chen, Guangcong Wang, Jiahao Zhu, Jianhuang Lai, and Xiaohua Xie. Guardsplat: Efficient and robust watermarking for 3d gaussian splatting. In *Proceedings of the Computer Vision and Pattern Recognition Conference*, pages 16325–16335, 2025.
- [17] Xiufeng Huang, Ziyuan Luo, Qi Song, Ruofei Wang, and Renjie Wan. Marksplat: Generalizable watermarking for 3d gaussian splatting model via splatter image structure. *arXiv preprint arXiv:2509.00757*, 2025.
- [18] Xuanyu Zhang, Jiarui Meng, Runyi Li, Zhipei Xu, Yongbing Zhang, and Jian Zhang. Gs-hider: Hiding messages into 3d gaussian splatting. *arXiv preprint arXiv:2405.15118*, 2024.
- [19] Xuanyu Zhang, Jiarui Meng, Zhipei Xu, Shuzhou Yang, Yanmin Wu, Ronggang Wang, and Jian Zhang. Securegs: Boosting the security and fidelity of 3d gaussian splatting steganography. *arXiv preprint arXiv:2503.06118*, 2025.

[20] Yan Ren, Shilin Lu, and Adams Wai-Kin Kong. All that glitters is not gold: Key-secured 3d secrets within 3d gaussian splatting. *arXiv preprint arXiv:2503.07191*, 2025.

[21] Chumeng Liang, Xiaoyu Wu, Yang Hua, Jiaru Zhang, Yiming Xue, Tao Song, Zhengui Xue, Ruhui Ma, and Haibing Guan. Adversarial example does good: Preventing painting imitation from diffusion models via adversarial examples. *arXiv preprint arXiv:2302.04578*, 2023.

[22] Haotian Xue, Chumeng Liang, Xiaoyu Wu, and Yongxin Chen. Toward effective protection against diffusion-based mimicry through score distillation. In *The Twelfth International Conference on Learning Representations*, 2024.

[23] Shawn Shan, Jenna Cryan, Emily Wenger, Haitao Zheng, Rana Hanocka, and Ben Y Zhao. Glaze: Protecting artists from style mimicry by {Text-to-Image} models. In *32nd USENIX Security Symposium (USENIX Security 23)*, pages 2187–2204, 2023.

[24] Hadi Salman, Alaa Khaddaj, Guillaume Leclerc, Andrew Ilyas, and Aleksander Madry. Raising the cost of malicious ai-powered image editing. *arXiv preprint arXiv:2302.06588*, 2023.

[25] Qianrui Teng, Xing Cui, Xuannan Liu, Peipei Li, Zekun Li, Huaibo Huang, and Ran He. Id-cloak: Crafting identity-specific cloaks against personalized text-to-image generation. *arXiv preprint arXiv:2502.08097*, 2025.

[26] Hanhui Wang, Yihua Zhang, Ruizheng Bai, Yue Zhao, Sijia Liu, and Zhengzhong Tu. Edit away and my face will not stay: Personal biometric defense against malicious generative editing. In *Proceedings of the Computer Vision and Pattern Recognition Conference*, pages 23806–23816, 2025.

[27] Ian J Goodfellow, Jonathon Shlens, and Christian Szegedy. Explaining and harnessing adversarial examples. *arXiv preprint arXiv:1412.6572*, 2014.

[28] Aleksander Madry, Aleksandar Makelov, Ludwig Schmidt, Dimitris Tsipras, and Adrian Vladu. Towards deep learning models resistant to adversarial attacks. *arXiv preprint arXiv:1706.06083*, 2017.

[29] Runyi Li, Xuanyu Zhang, Chuhan Tong, Zhipei Xu, and Jian Zhang. Gaussianseal: Rooting adaptive watermarks for 3d gaussian generation model. *arXiv preprint arXiv:2503.00531*, 2025.

[30] Sumin In, Youngdong Jang, Utae Jeong, MinHyuk Jang, Hyeongcheol Park, Eunbyung Park, and Sangpil Kim. Compmarkgs: Robust watermarking for compressed 3d gaussian splatting. *arXiv preprint arXiv:2503.12836*, 2025.

[31] Youngdong Jang, Hyunje Park, Feng Yang, Heejoo Ko, Euijin Choo, and Sangpil Kim. 3d-gsw: 3d gaussian splatting for robust watermarking. In *Proceedings of the Computer Vision and Pattern Recognition Conference*, pages 5938–5948, 2025.

[32] Junfeng Guo, Yiming Li, Lixu Wang, Shu-Tao Xia, Heng Huang, Cong Liu, and Bo Li. Domain watermark: Effective and harmless dataset copyright protection is closed at hand. *Advances in Neural Information Processing Systems*, 36:54421–54450, 2023.

[33] Lixu Wang, Shichao Xu, Ruiqi Xu, Xiao Wang, and Qi Zhu. Non-transferable learning: A new approach for model ownership verification and applicability authorization. *arXiv preprint arXiv:2106.06916*, 2021.

[34] Yiming Li, Shuo Shao, Yu He, Junfeng Guo, Tianwei Zhang, Zhan Qin, Pin-Yu Chen, Michael Backes, Philip Torr, Dacheng Tao, et al. Rethinking data protection in the (generative) artificial intelligence era. *arXiv preprint arXiv:2507.03034*, 2025.

[35] Ziming Hong, Yongli Xiang, and Tongliang Liu. Toward robust non-transferable learning: A survey and benchmark. *arXiv preprint arXiv:2502.13593*, 2025.

[36] Ziming Hong, Runnan Chen, Zengmao Wang, Bo Han, Bo Du, and Tongliang Liu. When data-free knowledge distillation meets non-transferable teacher: Escaping out-of-distribution trap is all you need. *arXiv preprint arXiv:2507.04119*, 2025.

[37] Ziming Hong, Li Shen, and Tongliang Liu. Your transferability barrier is fragile: Free-lunch for transferring the non-transferable learning. In *Proceedings of the IEEE/CVF Conference on Computer Vision and Pattern Recognition*, pages 28805–28815, 2024.

[38] Ziming Hong, Zhenyi Wang, Li Shen, Yu Yao, Zhuo Huang, Shiming Chen, Chuanwu Yang, Mingming Gong, and Tongliang Liu. Improving non-transferable representation learning by harnessing content and style. In *The twelfth international conference on learning representations*, 2024.

[39] Yongli Xiang, Ziming Hong, Lina Yao, Dadong Wang, and Tongliang Liu. Jailbreaking the non-transferable barrier via test-time data disguising. In *Proceedings of the Computer Vision and Pattern Recognition Conference*, pages 30671–30681, 2025.

[40] Cyrus Vachha and Ayaan Haque. Instruct-gs2gs: Editing 3d gaussian splats with instructions, 2024.

[41] Ruoxi Chen, Haibo Jin, Yixin Liu, Jinyin Chen, Haohan Wang, and Lichao Sun. Editshield: Protecting unauthorized image editing by instruction-guided diffusion models. In *European Conference on Computer Vision*, pages 126–142. Springer, 2024.

[42] Chumeng Liang and Xiaoyu Wu. Mist: Towards improved adversarial examples for diffusion models. *arXiv preprint arXiv:2305.12683*, 2023.

[43] Yixin Liu, Chenrui Fan, Yutong Dai, Xun Chen, Pan Zhou, and Lichao Sun. Metacloak: Preventing unauthorized subject-driven text-to-image diffusion-based synthesis via meta-learning. In *Proceedings of the IEEE/CVF Conference on Computer Vision and Pattern Recognition*, pages 24219–24228, 2024.

[44] Feifei Wang, Zhentao Tan, Tianyi Wei, Yue Wu, and Qidong Huang. Simac: A simple anti-customization method for protecting face privacy against text-to-image synthesis of diffusion models. In *Proceedings of the IEEE/CVF Conference on Computer Vision and Pattern Recognition*, pages 12047–12056, 2024.

[45] Chaojian Yu, Bo Han, Li Shen, Jun Yu, Chen Gong, Mingming Gong, and Tongliang Liu. Understanding robust overfitting of adversarial training and beyond. In *International Conference on Machine Learning*, pages 25595–25610. PMLR, 2022.

[46] Zhuo Huang, Xiaobo Xia, Li Shen, Bo Han, Mingming Gong, Chen Gong, and Tongliang Liu. Harnessing out-of-distribution examples via augmenting content and style. In *The Eleventh International Conference on Learning Representations*, 2023.

[47] Chaojian Yu, Bo Han, Mingming Gong, Li Shen, Shiming Ge, Bo Du, and Tongliang Liu. Robust weight perturbation for adversarial training. *arXiv preprint arXiv:2205.14826*, 2022.

[48] Chaojian Yu, Dawei Zhou, Li Shen, Jun Yu, Bo Han, Mingming Gong, Nannan Wang, and Tongliang Liu. Strength-adaptive adversarial training. *arXiv preprint arXiv:2210.01288*, 2022.

[49] Chaojian Yu, Xiaolong Shi, Jun Yu, Bo Han, and Tongliang Liu. Understanding robust overfitting from the feature generalization perspective. *arXiv preprint arXiv:2310.00607*, 2023.

[50] Wang Yifan, Felice Serena, Shihao Wu, Cengiz Öztïreli, and Olga Sorkine-Hornung. Differentiable surface splatting for point-based geometry processing. *ACM Transactions On Graphics (TOG)*, 38(6):1–14, 2019.

[51] Robin Rombach, Andreas Blattmann, Dominik Lorenz, Patrick Esser, and Björn Ommer. High-resolution image synthesis with latent diffusion models. In *Proceedings of the IEEE/CVF conference on computer vision and pattern recognition*, pages 10684–10695, 2022.

[52] Jing Wu, Jia-Wang Bian, Xinghui Li, Guangrun Wang, Ian Reid, Philip Torr, and Victor Adrian Prisacariu. Gaussctrl: Multi-view consistent text-driven 3d gaussian splatting editing. In *European Conference on Computer Vision*, pages 55–71. Springer, 2024.

[53] Yuxuan Wang, Xuanyu Yi, Zike Wu, Na Zhao, Long Chen, and Hanwang Zhang. View-consistent 3d editing with gaussian splatting. In *European Conference on Computer Vision*, pages 404–420. Springer, 2024.

[54] Jingyu Zhuang, Di Kang, Yan-Pei Cao, Guanbin Li, Liang Lin, and Ying Shan. Tip-editor: An accurate 3d editor following both text-prompts and image-prompts. *ACM Transactions on Graphics (TOG)*, 43(4):1–12, 2024.

[55] Junjie Wang, Jiemin Fang, Xiaopeng Zhang, Lingxi Xie, and Qi Tian. Gaussianeditor: Editing 3d gaussians delicately with text instructions. In *Proceedings of the IEEE/CVF conference on computer vision and pattern recognition*, pages 20902–20911, 2024.

[56] Huanran Chen, Yinpeng Dong, Shitong Shao, Hao Zhongkai, Xiao Yang, Hang Su, and Jun Zhu. Diffusion models are certifiably robust classifiers. *Advances in Neural Information Processing Systems*, 37:50062–50097, 2024.

[57] Haotian Xue and Yongxin Chen. Pixel is a barrier: Diffusion models are more adversarially robust than we think. *arXiv preprint arXiv:2404.13320*, 2024.

[58] Alexander Kirillov, Eric Mintun, Nikhila Ravi, Hanzi Mao, Chloe Rolland, Laura Gustafson, Tete Xiao, Spencer Whitehead, Alexander C. Berg, Wan-Yen Lo, Piotr Dollár, and Ross Girshick. Segment anything. *arXiv:2304.02643*, 2023.

[59] Ayaan Haque, Matthew Tancik, Alexei A Efros, Aleksander Holynski, and Angjoo Kanazawa. Instruct-nerf2nerf: Editing 3d scenes with instructions. In *Proceedings of the IEEE/CVF International Conference on Computer Vision*, pages 19740–19750, 2023.

[60] Can Wang, Ruixiang Jiang, Menglei Chai, Mingming He, Dongdong Chen, and Jing Liao. Nerf-art: Text-driven neural radiance fields stylization. *IEEE Transactions on Visualization and Computer Graphics*, 30(8):4983–4996, 2023.

[61] Yao Yao, Zixin Luo, Shiwei Li, Jingyang Zhang, Yufan Ren, Lei Zhou, Tian Fang, and Long Quan. Blendedmvs: A large-scale dataset for generalized multi-view stereo networks. In *Proceedings of the IEEE/CVF conference on computer vision and pattern recognition*, pages 1790–1799, 2020.

[62] Zhou Wang, Alan C Bovik, Hamid R Sheikh, and Eero P Simoncelli. Image quality assessment: from error visibility to structural similarity. *IEEE transactions on image processing*, 13(4):600–612, 2004.

[63] Richard Zhang, Phillip Isola, Alexei A Efros, Eli Shechtman, and Oliver Wang. The unreasonable effectiveness of deep features as a perceptual metric. In *Proceedings of the IEEE conference on computer vision and pattern recognition*, pages 586–595, 2018.

[64] Andrew Ilyas, Shibani Santurkar, Dimitris Tsipras, Logan Engstrom, Brandon Tran, and Aleksander Madry. Adversarial examples are not bugs, they are features. *Advances in neural information processing systems*, 32, 2019.

[65] Cihang Xie, Yuxin Wu, Laurens van der Maaten, Alan L Yuille, and Kaiming He. Feature denoising for improving adversarial robustness. In *Proceedings of the IEEE/CVF conference on computer vision and pattern recognition*, pages 501–509, 2019.

[66] Sara Sabour, Yanshuai Cao, Fartash Faghri, and David J Fleet. Adversarial manipulation of deep representations. *arXiv preprint arXiv:1511.05122*, 2015.

[67] Martin Heusel, Hubert Ramsauer, Thomas Unterthiner, Bernhard Nessler, and Sepp Hochreiter. Gans trained by a two time-scale update rule converge to a local nash equilibrium. *Advances in neural information processing systems*, 30, 2017.

[68] Mehdi SM Sajjadi, Olivier Bachem, Mario Lucic, Olivier Bousquet, and Sylvain Gelly. Assessing generative models via precision and recall. *Advances in neural information processing systems*, 31, 2018.

[69] Kai Zhang, Lingbo Mo, Wenhui Chen, Huan Sun, and Yu Su. Magicbrush: A manually annotated dataset for instruction-guided image editing. *Advances in Neural Information Processing Systems*, 36:31428–31449, 2023.

[70] Chenlin Meng, Yutong He, Yang Song, Jiaming Song, Jiajun Wu, Jun-Yan Zhu, and Stefano Ermon. Sdedit: Guided image synthesis and editing with stochastic differential equations. *arXiv preprint arXiv:2108.01073*, 2021.

[71] Dustin Podell, Zion English, Kyle Lacey, Andreas Blattmann, Tim Dockhorn, Jonas Müller, Joe Penna, and Robin Rombach. Sdxl: Improving latent diffusion models for high-resolution image synthesis. *arXiv preprint arXiv:2307.01952*, 2023.

[72] Weili Nie, Brandon Guo, Yujia Huang, Chaowei Xiao, Arash Vahdat, and Anima Anandkumar. Diffusion models for adversarial purification. *arXiv preprint arXiv:2205.07460*, 2022.

[73] Pedro Sandoval-Segura, Jonas Geiping, and Tom Goldstein. Jpeg compressed images can bypass protections against ai editing. *arXiv preprint arXiv:2304.02234*, 2023.

Appendices:

- Appendix A: Comparing training dynamic for Fit2D, and different variants of AdLift.
- Appendix B: Comparison with soft constraint methods for learning 3DGS perturbations.
- Appendix C: More qualitative and quantitative results of AdLift.
- Appendix D: Robustness to editing hyperparameters.
- Appendix E: Analysis of AdLift hyperparameters.
- Appendix F: Transferability, robustness, and generality of AdLift.
- Appendix G: More discussion and limitation.
- Appendix H: More experimental details and the full editing instructions.

A Training Dynamics

Figure 9 compares the training dynamics of directly fitting 2D views individually protected with adversarial perturbations (denoted as Fit2D) and our AdLift variants, where higher adversarial loss indicates stronger attack strength. As discussed in the introduction, directly optimizing perturbations in the 2D domain suffers from view-specific conflicts, which cause underfitting on training views and poor generalization to novel views. As a result, Fit2D yields only limited improvement in adversarial loss even after prolonged training. By contrast, our Lifted-PGD-based strategy quickly enhances the adversarial loss on both training and novel views, demonstrating its ability to achieve view-generalizable protection. Moreover, initializing AdLift* from a pretrained Fit2D model yields consistently higher protection strength compared to applying AdLift directly on raw assets, highlighting the benefit of warm-starting with 2D guidance. Nevertheless, even without such initialization, AdLift significantly outperforms direct 2D fitting, confirming that lifting adversarial perturbations into the 3D Gaussian space is crucial for achieving both effectiveness and cross-view consistency.

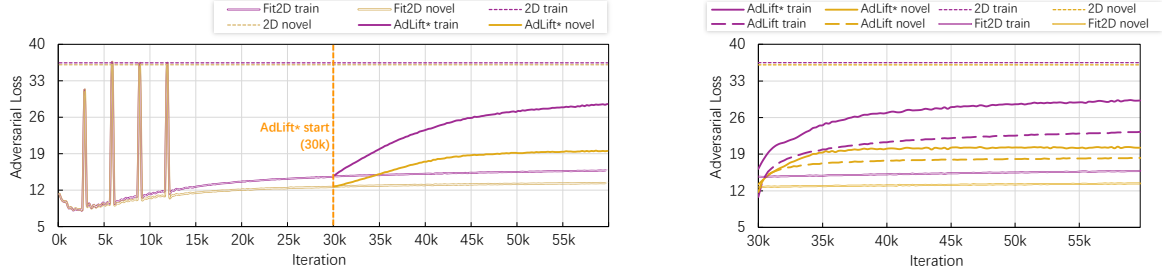


Figure 9: Training dynamic of Fit2D, AdLift, and AdLift* with VAE-untargeted loss \mathcal{L}_{VU} .

B Soft Constraint on Gaussians Parameters

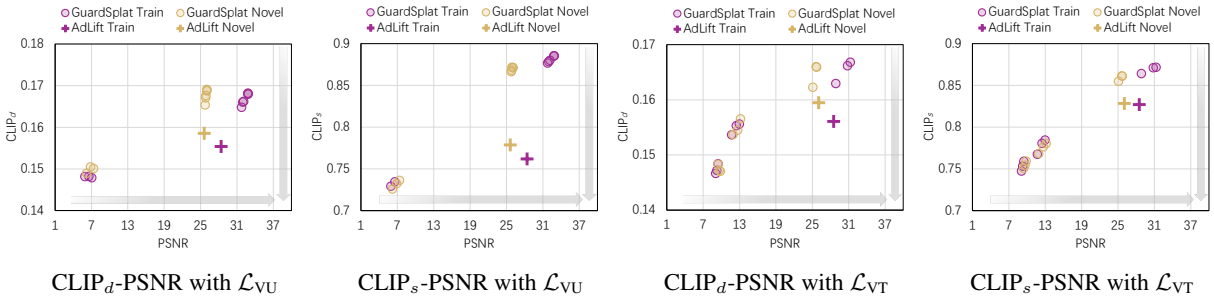


Figure 10: Comparison of balance between imperceptibility and protection capability. We show CLIP_d -PSNR scatter plot and CLIP_s -PSNR scatter plot on both GuardSplat and AdLift trained by VAE-targeted loss \mathcal{L}_{VT} and VAE-untargeted loss \mathcal{L}_{VU} . (Lower CLIP_d / CLIP_s indicates stronger protection, while higher PSNR reflects better imperceptibility).

Figures 10 and 11 compare our AdLift with GuardSplat [16], which perturbs the spherical-harmonic (SH) features of Gaussians under soft invisibility regularization (e.g., SSIM). As shown in Figure 10, GuardSplat struggles to balance

imperceptibility and protection: achieving stronger protection inevitably sacrifices imperceptibility, while preserving fidelity leads to weak protection. In contrast, our AdLift enforces strict bounds in the rendering space, achieving lower CLIP and higher PSNR simultaneously, thus reaching a much better trade-off. Besides, step-wise visualizations in Figure 11 further confirm this: GuardSplat accumulates severe color distortions due to perturbed SH features, whereas AdLift preserves natural appearance while still suppressing instruction-driven edits. These results verify that soft constraints on SH features cannot reach a satisfactory balance, underscoring the necessity of our strictly bounded constraints. More quantitative and qualitative results are shown in Appendix F.1.

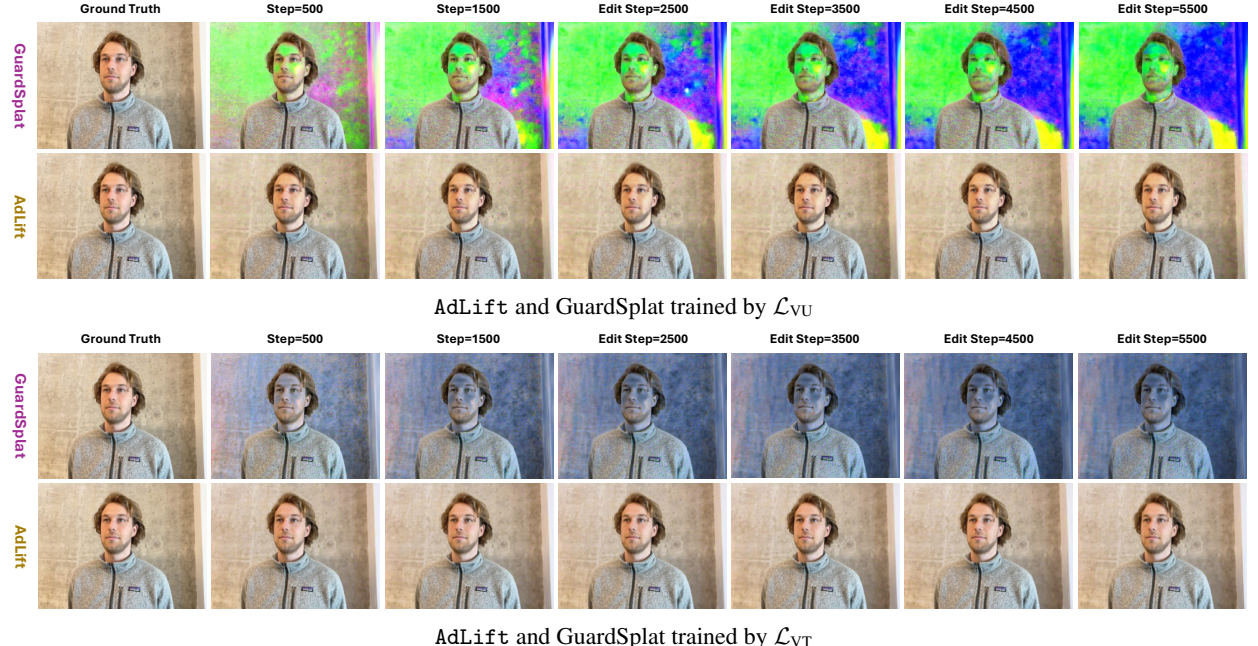


Figure 11: Step-wise comparison of balance between imperceptibility and protection capability. We show visualization results of our AdLift and GuardSplat [16] trained by VAE-targeted loss \mathcal{L}_{VT} and VAE-untargeted loss \mathcal{L}_{VU} .

C More Qualitative and Quantitative Results of AdLift

C.1 Visualization of learned perturbations.

Figure 12 shows the protection perturbations produced by AdLift* on bear and stone-horse scenes. The perturbations remain consistent across different viewpoints, indicating strong cross-view continuity rather than view-specific noise. Moreover, the perturbations exhibit structured, semantically aligned patterns (e.g., contours along object boundaries and textures), instead of appearing as purely random pixel-level noise. Such properties highlight that the learned perturbations are not arbitrary but encode meaningful adversarial signals [64, 65, 66] that generalize across views.

C.2 More Results on Instruction-based Image Editing

Figure 14 presents qualitative comparisons of unprotected and protected 3DGS assets under instruction-driven 2D editing with IP2P [11]. For both training and novel views, unprotected assets are highly vulnerable: IP2P faithfully executes the editing instructions, producing drastic manipulations such as adding moustaches, changing background scenes, or altering facial attributes. By contrast, assets protected with our AdLift exhibit strong resistance to these instruction-based edits. Across both Face and Fangzhou scenes, the protected assets fail to produce realistic editing outcomes under given instructions. While unprotected assets can be directly edited to follow instructions with faithful preservation of facial structures, the protected results instead appear unnatural and deviate from photorealism, effectively preventing meaningful semantic modifications. Notably, this protection generalizes from training views to novel views, confirming that our lifted perturbations enforce view-consistent protection rather than overfitting to the supervised views. These results validate that AdLift provides effective and generalizable safeguards against instruction-guided editing attacks.



Figure 12: Visualization of protection perturbations learned via AdLift*-VU.

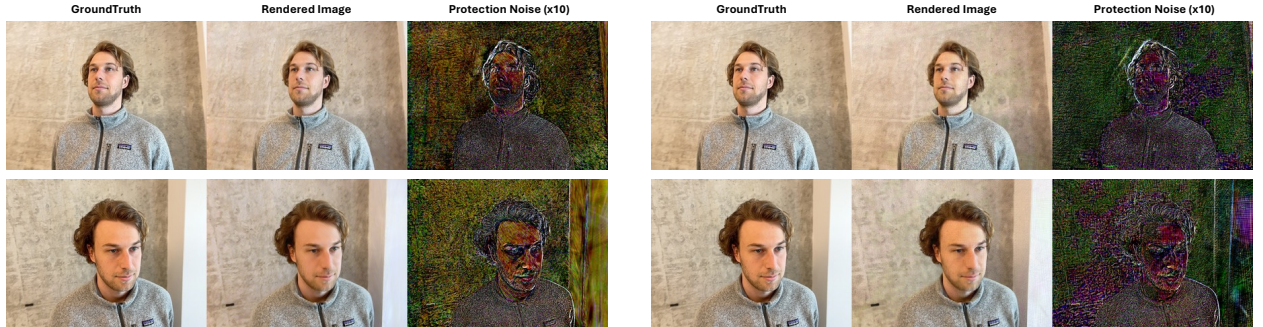


Figure 13: Visualization the learned perturbations of AdLift* trained via different adversarial losses. (*Left*): AdLift* with targeted VAE loss. (*Right*): AdLift* with untargeted VAE loss.

Beside, the full quantitative results on each scenes are shown in Table 3, with Figure 15 qualitatively comparing different protection variants. In details, random noise fails to provide effective defense, as edits are still successfully applied. Fit2D variants partially suppress editing, but the protection is view-inconsistent and often leaves residual manipulations in novel views. In contrast, our AdLift variants achieve much stronger and more stable protection.

C.3 More Results on Instruction-based 3DGS Editing

The full quantitative results of instruction-based 3DGS global editing and local editing are shown in Table 4 and Table 5, respectively. In addition, we show more qualitative results in Figure 16. Our AdLift disrupts both global and local instruction-driven 3DGS edits, either by preventing intended transformations or by misguiding region localization to preserve the original appearance.

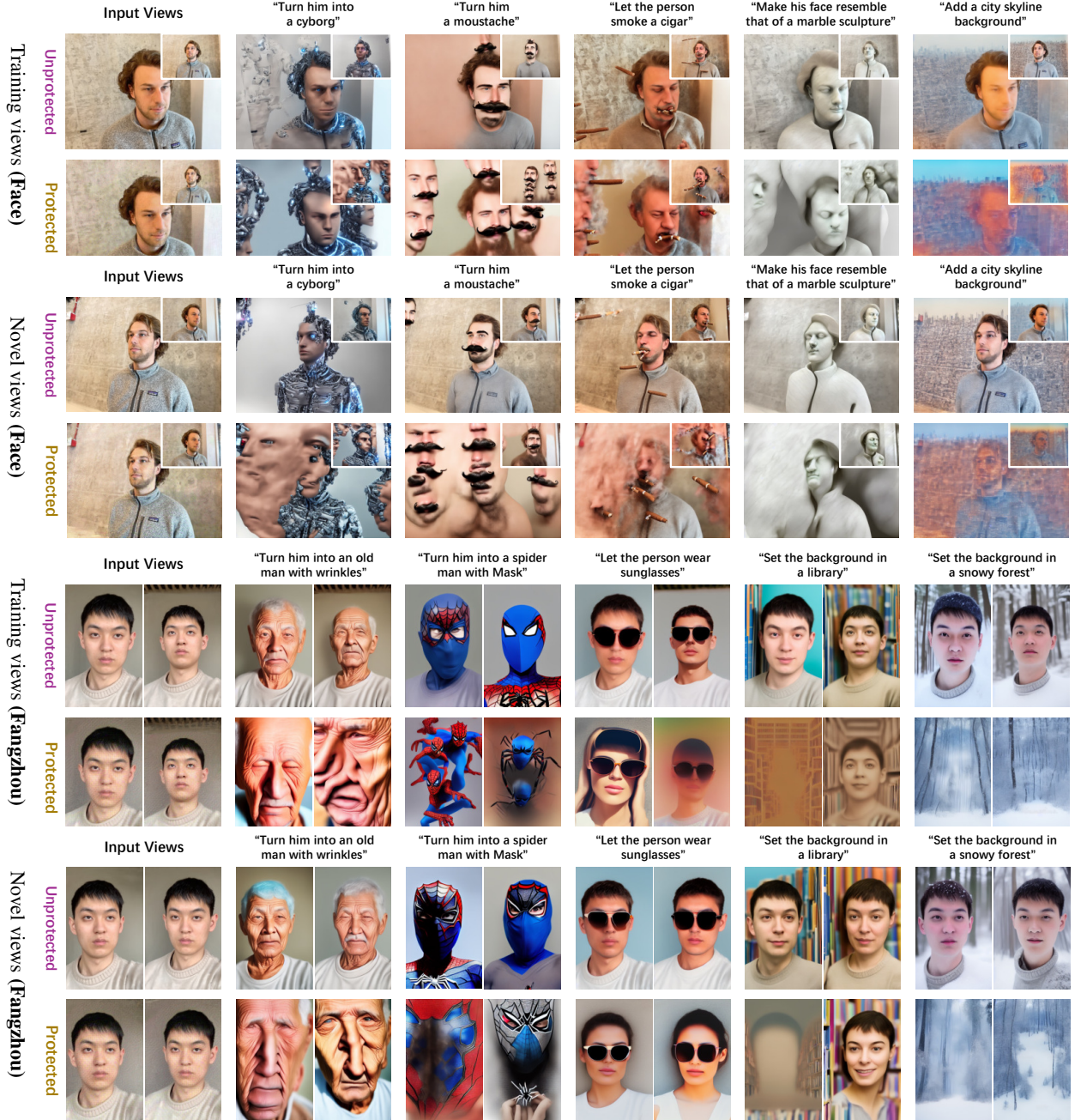


Figure 14: Qualitative results of instruction-based image editing on face scenes. We show the comparison of editing results of unprotected 3D assets and 3D assets protected by AdLift*-VU.

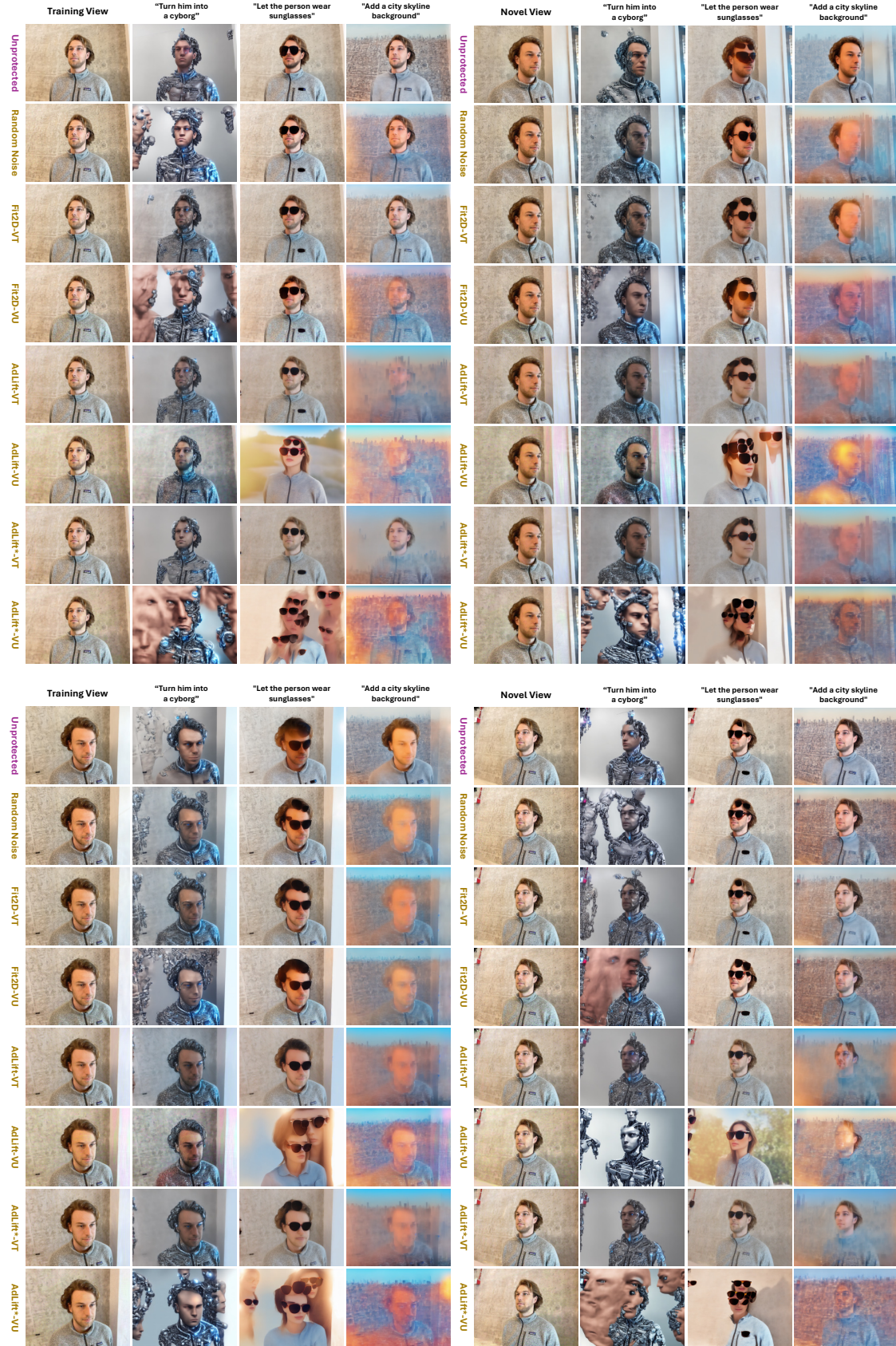


Figure 15: Visualization results of different variants of protection.

Table 3: Quantitative evaluations on instruction-based image editing. We report results on both training and novel views. For invisibility, higher SSIM and PSNR, and lower LPIPS indicate better fidelity to the original image. For protection quality, lower CLIP_d and CLIP_s suggests stronger resistance to view-dependent instruction-based editing.

Dataset	Method	Training Views					Novel Views				
		Invisibility			Protection Quality		Invisibility			Protection Quality	
		SSIM(↑)	PSNR(↑)	LPIPS(↓)	CLIP _d (↓)	CLIP _s (↓)	SSIM(↑)	PSNR(↑)	LPIPS(↓)	CLIP _d (↓)	CLIP _s (↓)
Face	Ground Truth	—	—	—	0.1688	—	—	—	—	0.1715	—
	No Protection	0.9381	32.6436	0.0668	0.1685	0.8852	0.8590	26.0390	0.1292	0.1704	0.8730
	Random Noise	0.7810	28.3994	0.1785	0.1607	0.8578	0.7126	25.3380	0.2147	0.1623	0.8512
	Fit2D-VU	0.7446	28.4200	0.2811	0.1542	0.8192	0.6601	25.1338	0.3103	0.1564	0.8165
	Fit2D-VT	0.8346	29.5256	0.1547	0.1567	0.8515	0.7575	26.2201	0.1960	0.1591	0.8532
	AdLift-VU	0.7488	28.6118	0.3308	0.1561	0.7990	0.6764	24.4293	0.3718	0.1572	0.7998
	AdLift-VT	0.8075	28.6309	0.2011	0.1574	0.8326	0.7340	24.5285	0.2552	0.1591	0.8272
	AdLift*-VU	0.7001	28.3963	0.3774	0.1554	0.7620	0.6367	25.6115	0.4018	0.1586	0.7786
	AdLift*-VT	0.7842	28.5198	0.2250	0.1561	0.8272	0.7239	26.0586	0.2522	0.1595	0.8285
Fang-zhou	Ground Truth	—	—	—	0.2016	—	—	—	—	0.2004	—
	No Protection	0.9218	32.1021	0.1093	0.1937	0.9080	0.9010	30.2873	0.1161	0.1938	0.9053
	Random Noise	0.7073	27.9112	0.1995	0.1955	0.8899	0.6849	26.9362	0.2107	0.1944	0.8867
	Fit2D-VU	0.7164	28.4063	0.2976	0.1919	0.8595	0.6853	27.3809	0.3116	0.1937	0.8952
	Fit2D-VT	0.8415	29.6154	0.1442	0.1883	0.8801	0.8163	28.3239	0.1574	0.1890	0.8796
	AdLift-VU	0.7386	28.5668	0.2783	0.1770	0.8090	0.7245	27.6556	0.2829	0.1783	0.8092
	AdLift-VT	0.8142	28.6419	0.1916	0.1792	0.8314	0.8021	27.8007	0.1972	0.1805	0.8290
	AdLift*-VU	0.6706	28.3497	0.3767	0.1781	0.7900	0.6550	27.4526	0.3762	0.1791	0.8037
	AdLift*-VT	0.8009	28.6429	0.2156	0.1776	0.8198	0.7903	27.6700	0.2205	0.1788	0.8148
Bear	Ground Truth	—	—	—	0.1858	—	—	—	—	0.1863	—
	No Protection	0.9111	27.0824	0.0885	0.1852	0.8734	0.7623	21.2934	0.1800	0.1856	0.8626
	Random Noise	0.8048	24.8107	0.1545	0.1806	0.8575	0.6793	20.4670	0.2342	0.1836	0.8527
	Fit2D-VU	0.8241	25.0807	0.2042	0.1785	0.8407	0.6844	20.5878	0.2792	0.1786	0.8394
	Fit2D-VT	0.8349	25.4106	0.1433	0.1718	0.8411	0.6916	20.7411	0.2281	0.1726	0.8361
	AdLift-VU	0.8401	26.1373	0.1835	0.1849	0.8373	0.7100	21.0489	0.2595	0.1851	0.8336
	AdLift-VT	0.8353	26.1047	0.1402	0.1777	0.8402	0.7061	21.0953	0.2201	0.1774	0.8342
	AdLift*-VU	0.8081	25.7041	0.2145	0.1865	0.8232	0.6755	20.6248	0.2924	0.1833	0.8306
	AdLift*-VT	0.8092	25.8351	0.1541	0.1769	0.8291	0.6782	20.7417	0.2401	0.1723	0.8253
Horse	Ground Truth	—	—	—	0.2043	—	—	—	—	0.2138	—
	No Protection	0.9149	30.0968	0.0575	0.2025	0.8903	0.7019	22.5986	0.1033	0.2105	0.8865
	Random Noise	0.7055	25.7536	0.1581	0.1944	0.8694	0.5492	21.4967	0.1882	0.2050	0.8660
	Fit2D-VU	0.7375	26.3795	0.2433	0.1941	0.8276	0.5615	21.7023	0.2515	0.2014	0.8439
	Fit2D-VT	0.7817	27.1458	0.1311	0.1838	0.8538	0.6016	21.9937	0.1660	0.1984	0.8679
	AdLift-VU	0.7730	27.6010	0.2185	0.1967	0.8102	0.6097	22.0334	0.2223	0.1989	0.8297
	AdLift-VT	0.7963	27.8463	0.1352	0.1848	0.8439	0.6305	22.1679	0.1656	0.1959	0.8560
	AdLift*-VU	0.7332	27.1573	0.2589	0.2023	0.7804	0.5822	21.9479	0.2615	0.1996	0.8217
	AdLift*-VT	0.7642	27.4353	0.1445	0.1819	0.8271	0.6106	21.8557	0.1830	0.1927	0.8496

Table 4: Quantitative evaluations on instruction-based global 3DGS editing. We report results on both training and novel views on four scenes.

Dataset	Method	Instruct-GS2GS				DGE (Global)			
		Training Views		Novel Views		Training Views		Novel Views	
		CLIP _d (\downarrow)	CLIP _s (\downarrow)	CLIP _d (\downarrow)	CLIP _s (\downarrow)	CLIP _d (\downarrow)	CLIP _s (\downarrow)	CLIP _d (\downarrow)	CLIP _s (\downarrow)
Face	No Protection	0.1239	—	0.1108	—	0.1240	—	0.1218	—
	AdLift*-VT	0.1138	0.8758	0.1031	0.8682	0.1162	0.9300	0.1166	0.9298
	AdLift*-VU	0.1107	0.7914	0.0857	0.8046	0.1154	0.8986	0.1200	0.9029
Fangzhou	No Protection	0.1339	—	0.1324	—	0.1710	—	0.1713	—
	AdLift*-VT	0.1151	0.8734	0.1119	0.87305	0.1431	0.8877	0.1432	0.8875
	AdLift*-VU	0.1194	0.8269	0.1160	0.8259	0.1523	0.8633	0.1522	0.8630
Bear	No Protection	0.1351	—	0.1273	—	0.1025	—	0.1009	—
	AdLift*-VT	0.1484	0.8483	0.1292	0.8529	0.0901	0.9398	0.0890	0.9400
	AdLift*-VU	0.1386	0.8886	0.1236	0.8951	0.0911	0.9318	0.0897	0.9308
Horse	No Protection	0.1557	—	0.1300	—	0.1174	—	0.1243	—
	AdLift*-VT	0.1512	0.8683	0.1223	0.8831	0.1088	0.9301	0.1160	0.9341
	AdLift*-VU	0.1806	0.8033	0.1468	0.8029	0.1037	0.9157	0.1086	0.9179

Table 5: Quantitative evaluations on instruction-based 3DGS local editing

Dataset	Method	DGE (Local)			
		Training Views		Novel Views	
		CLIP _d (\downarrow)	CLIP _s (\downarrow)	CLIP _d (\downarrow)	CLIP _s (\downarrow)
Face	No Protection	0.1377	—	0.13329	—
	AdLift-ST	0.0574	0.8606	0.0691	0.8712
Fangzhou	No Protection	0.2000	—	0.1951	—
	AdLift-ST	0.0300	0.8014	0.0236	0.7984
Bear	No Protection	0.0946	—	0.0979	—
	AdLift-ST	-0.0040	0.86752	0.0026	0.8615
Horse	No Protection	0.1024	—	0.1022	—
	AdLift-ST	0.0721	0.9076	0.0746	0.9160



Figure 16: Multi view visualization for protection against instruction-based 3DGS local editing.

D Robustness to Editing Hyperparameters

An important requirement for practical protection is robustness against variations in editing hyperparameters, since adversaries can freely adjust parameters of instruction-driven editing models. To evaluate this, we evaluate our AdLift under different settings of `guidance_scale`, `image_guidance_scale`, and `num_inference_steps`.

Guidance Scale. As shown in Figure 17, increasing the `guidance_scale` generally strengthens the editing effect on unprotected assets, leading to higher CLIP_d and CLIP_s scores. In contrast, our protected assets maintain consistently low of both CLIP scores across a wide range of values. This indicates that AdLift provides stable protection even when the editing strength is increased.

Image Guidance Scale. As shown in Figure 18, our protection demonstrates superiority, consistently achieving lower CLIP_d and CLIP_s scores and thus stronger resistance for a wide range of `image_guidance_scale`. However, extreme values of `image_guidance_scale` (either too small or too large) render the editing itself ineffective.

Number of Inference Steps. Figure 19 shows results under different numbers of diffusion inference steps. Although both the CLIP_d and CLIP_s scores increase as the number of steps increases, the gap compared to unprotected assets remains substantial, illustrating the effectiveness of AdLift under varying editing steps.

In addition, we provide visualizations under different editing hyperparameters in Figures 17 to 19, which further verify the effectiveness and stability of our method across diverse editing configurations. Overall, across all tested hyperparameters, AdLift consistently outperforms baselines, yielding lower CLIP_d and CLIP_s on both training and novel views. These results highlight that our protection is not tied to specific editing settings, but instead provides strong and generalizable robustness against diverse editing configurations.

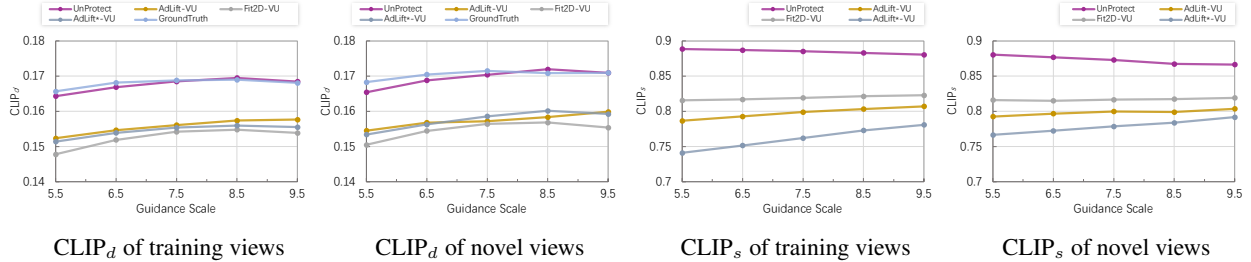


Figure 17: The robustness of AdLift against different `guidance_scale` in *instruction-based image editing* (fixing `num_inference_steps`=10, `image_guidance_scale`=1.0). Smaller CLIP_d and CLIP_s indicate better resistance against instruction-based image editing.

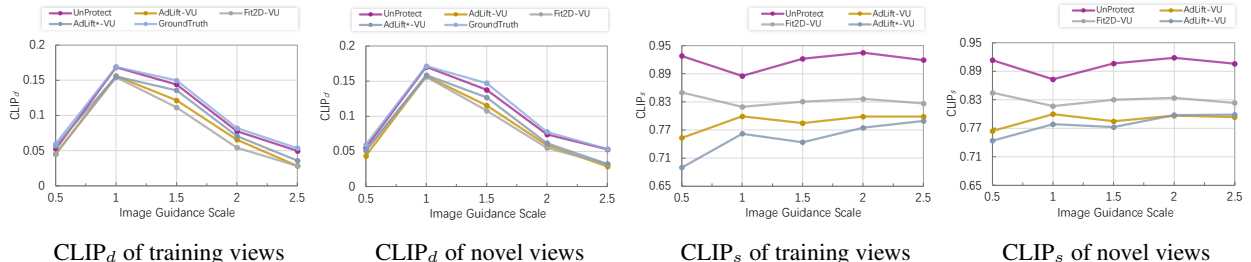


Figure 18: The robustness of AdLift against different `image_guidance_scale` in *instruction-based image editing* (fixing `num_inference_steps`=10, `guidance_scale`=7.5). Smaller CLIP_d and CLIP_s indicate better resistance against instruction-based image editing.

E Analysis of Different Protection Hyperparameters

Figures 23 to 26 analyze the influence of different training hyperparameters for AdLift*, including the perturbation budget η , learning rate α , gradient truncation steps K_p , and image-to-Gaussian fitting steps K_l . From the results, the perturbation budget η plays the most critical role: larger η significantly enhances protection strength (lower $\text{CLIP}_d/\text{CLIP}_s$), but at the cost of noticeable degradation in visual quality (lower SSIM/PSNR, higher LPIPS). This indicates a clear trade-off between imperceptibility and protection effectiveness, and choosing an appropriate budget is essential in practice. In contrast, other hyperparameters have only minor influence, with protection and fidelity metrics remaining largely stable across different settings.

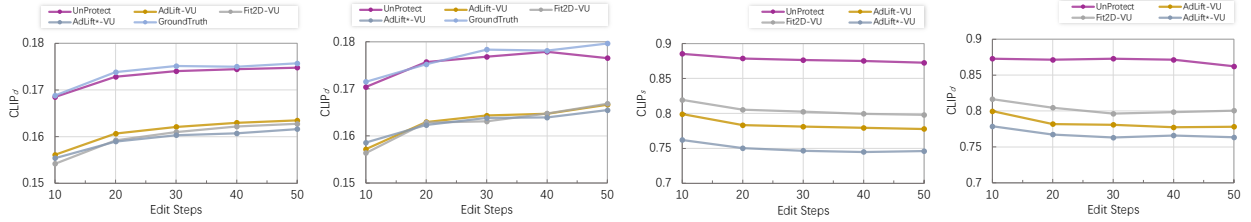


Figure 19: The robustness of AdLift against different `num_inference_steps` in *instruction-based image editing* (fixing `image_guidance_scale`=1.0, `guidance_scale`=7.5). Smaller CLIP_d and CLIP_s indicate better resistance against instruction-based image editing.



Figure 20: Visualization results of different editing `guidance_scale`. We edit unprotected 3DGS assets and 3DGS assets protected by AdLift*-VU.



Figure 21: Visualization results of different editing `image_guidance_scale`. We edit unprotected 3DGS assets and 3DGS assets protected by AdLift*-VU.



Figure 22: Visualization results of different editing `num_inference_steps`. We edit unprotected 3DGS assets and 3DGS assets protected by AdLift*-VU.

We also show visualization results of editing protected 3DGS assets by AdLift with different budgets in Figure 27, which further illustrate the trade-off between imperceptibility and protection effectiveness. These qualitative comparisons are consistent with our quantitative analysis.

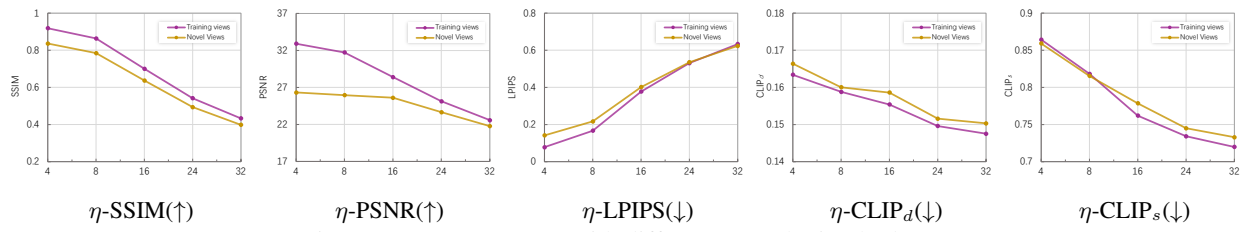


Figure 23: AdLift*-VU with different perturbation budget η .

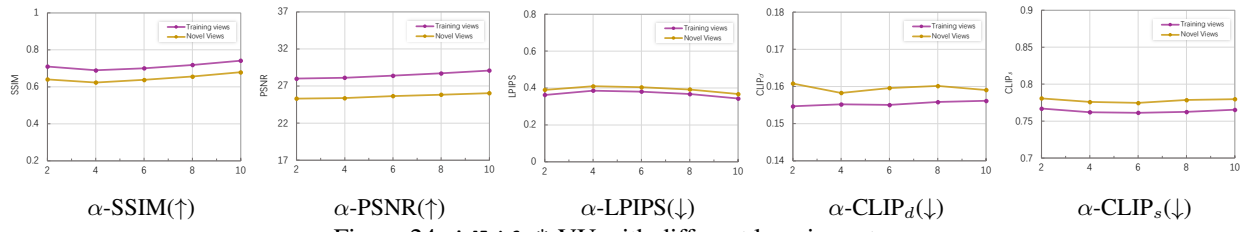


Figure 24: AdLift*-VU with different learning rate α .

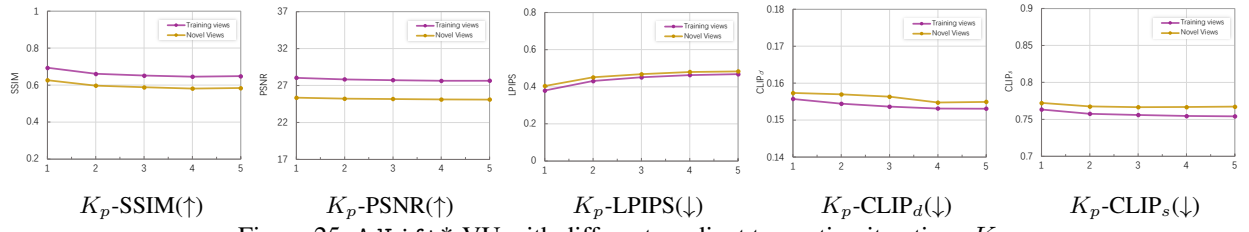
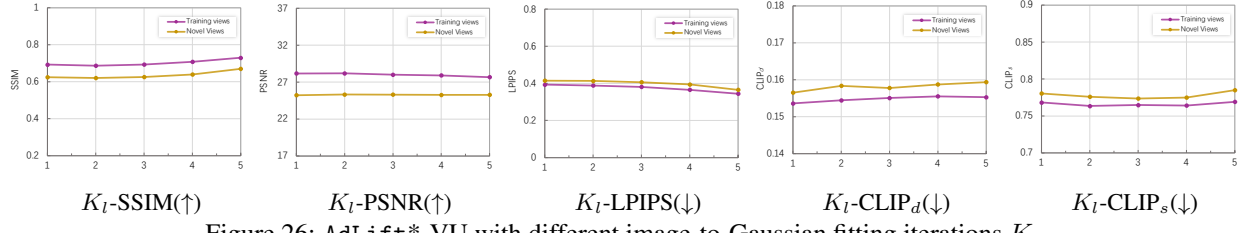
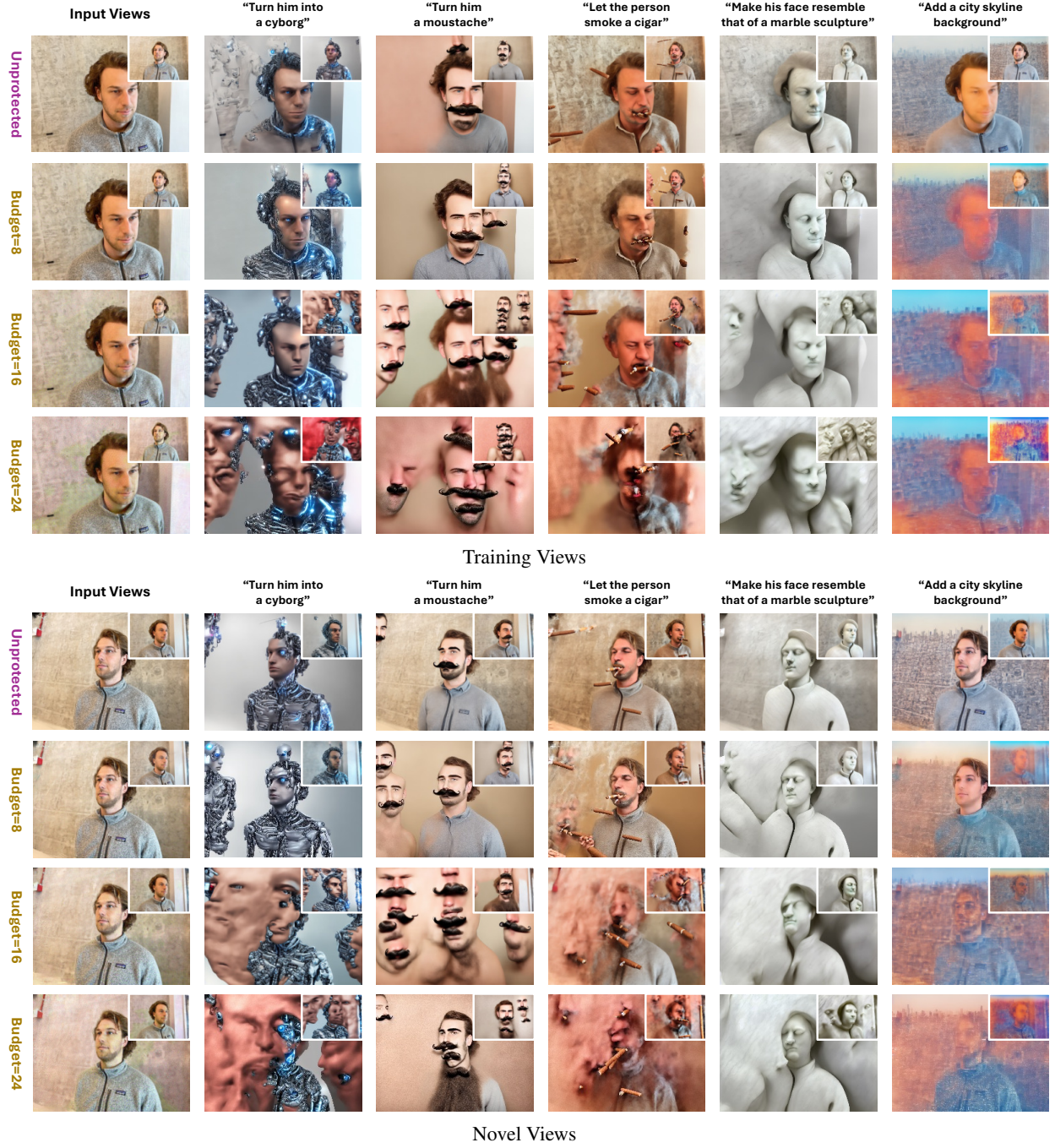


Figure 25: AdLift*-VU with different gradient truncation iterations K_p .

Figure 26: AdLift*-VU with different image-to-Gaussian fitting iterations K_l .Figure 27: Visualization results of different perturbation budget η . We show editing results of unprotected 3DGS assets and 3DGS assets protected by AdLift*-VU.

F Transferability, Robustness, and Generality of AdLift

E.1 More Comprehensive Comparison with Soft-constraint Baselines

Comparison with GuardSplat at matched PSNR or protection levels. We provide both quantitative and qualitative comparisons between AdLift and GuardSplat [16] under matched PSNR or protection levels. The quantitative results are reported in Tables 6 and 7, which include: (i) comparisons under similar PSNR levels (GuardSplat-VU1 vs. AdLift-VU), and (ii) comparisons under similar anti-editing performance with matched perceptual quality (GuardSplat-VU2 vs. AdLift-VU). We also report the adversarial loss values along with the additional three editing metrics (FID [67], $F_{1/8}$, and F_8 [68]). Qualitative editing results comparing AdLift and GuardSplat at the same PSNR levels are shown in Figures 28 and 29.

Overall, the quantitative and qualitative results consistently confirm that AdLift better balances imperceptibility and protection effectiveness: under matched PSNR levels AdLift delivers stronger editing resistance, and under matched protection strength it maintains higher perceptual quality compared to GuardSplat-based baselines.

Table 6: Comparison with GuardSplat at the same PSNR-level or anti-editing-level (Face).

Method	SSIM (\uparrow)	PSNR (\uparrow)	LPIPS (\downarrow)	CLIP _d (\downarrow)	CLIP _s (\downarrow)	AdvLoss (\uparrow)	FID (\uparrow)	$F_{1/8}$ (\downarrow)	F_8 (\downarrow)
Training views									
No Protection	0.9381	32.6436	0.0668	0.1685	0.8852	–	22.0270	0.9958	0.9947
GuardSplat-VU1	0.9348	31.7765	0.0802	0.1649	0.8769	5.4381	26.2044	0.9945	0.9952
GuardSplat-VU2	0.4855	7.0444	0.6414	0.1479	0.7387	51.6294	126.1376	0.7694	0.6478
AdLift*-VU	0.7001	28.3963	0.3774	0.1554	0.7620	29.2730	88.5865	0.8954	0.8742
Novel views									
No Protection	0.8590	26.0390	0.1292	0.1704	0.8730	–	76.2210	0.9882	0.9835
GuardSplat-VU1	0.8552	25.7744	0.1442	0.1654	0.8666	6.3217	83.8178	0.9846	0.9875
GuardSplat-VU2	0.4328	7.3565	0.6576	0.1501	0.7361	47.7983	176.4602	0.7253	0.5904
AdLift*-VU	0.6367	25.6115	0.4018	0.1586	0.7786	20.2232	129.8172	0.8807	0.9279

Table 7: Comparison with GuardSplat at the same PSNR-level or anti-editing-level (Fangzhou).

Method	SSIM (\uparrow)	PSNR (\uparrow)	LPIPS (\downarrow)	CLIP _d (\downarrow)	CLIP _s (\downarrow)	AdvLoss (\uparrow)	FID (\uparrow)	$F_{1/8}$ (\downarrow)	F_8 (\downarrow)
Training views									
No Protection	0.9218	32.1021	0.1093	0.1937	0.9080	–	23.7996	0.9817	0.9795
GuardSplat-VU1	0.8596	23.4021	0.2126	0.1874	0.8380	18.4520	53.6308	0.9248	0.9653
GuardSplat-VU2	0.3850	6.4662	0.6600	0.1727	0.7432	58.1082	121.3719	0.6165	0.4988
AdLift*-VU	0.6706	28.3497	0.3767	0.1781	0.7900	29.4458	84.2180	0.8030	0.7749
Novel views									
No Protection	0.9010	30.2873	0.1161	0.1938	0.9053	–	51.7357	0.9905	0.9913
GuardSplat-VU1	0.8396	22.8568	0.2201	0.1904	0.8339	18.0344	87.1272	0.9270	0.9481
GuardSplat-VU2	0.3765	6.4916	0.6594	0.1722	0.7374	56.8699	151.8966	0.6272	0.4956
AdLift*-VU	0.6550	27.4526	0.3762	0.1791	0.8037	24.3330	102.6782	0.8337	0.8794

Comparison with more baselines at the matched PSNR level. We additionally include several potential baselines by adapting representative 3DGS watermarking methods into an adversarial training regime, and compare them against AdLift under matched perceptual quality. Specifically, we include the following variants:

- GuardSplat-(SH): Perturb only the Spherical-Harmonic (SH) features of all Gaussians, following the original GuardSplat [16] design.
- GuardSplat-(PC): Perturb Positions and Covariance features of all Gaussians using GuardSplat [16].
- GuardSplat-(Full): Perturb all features of all Gaussians using GuardSplat [16], including: Position, Covariance, Opacity, and SH features.
- GaussianMarker [15]: Split low-uncertainty Gaussians and optimize the newly added Gaussians to encode perturbations.

For each method, we evaluate two adversarial objectives, untargeted VAE loss (VU) and targeted VAE loss (VT), to ensure comparison under different attack settings. We preserve each method’s original fidelity-preserving loss but



Figure 28: Comparison of qualitative editing results for GuardSplat-VU (with 2 different configurations) and AdLift*-VU at the same PSNR-level or anti-editing-level (Face).

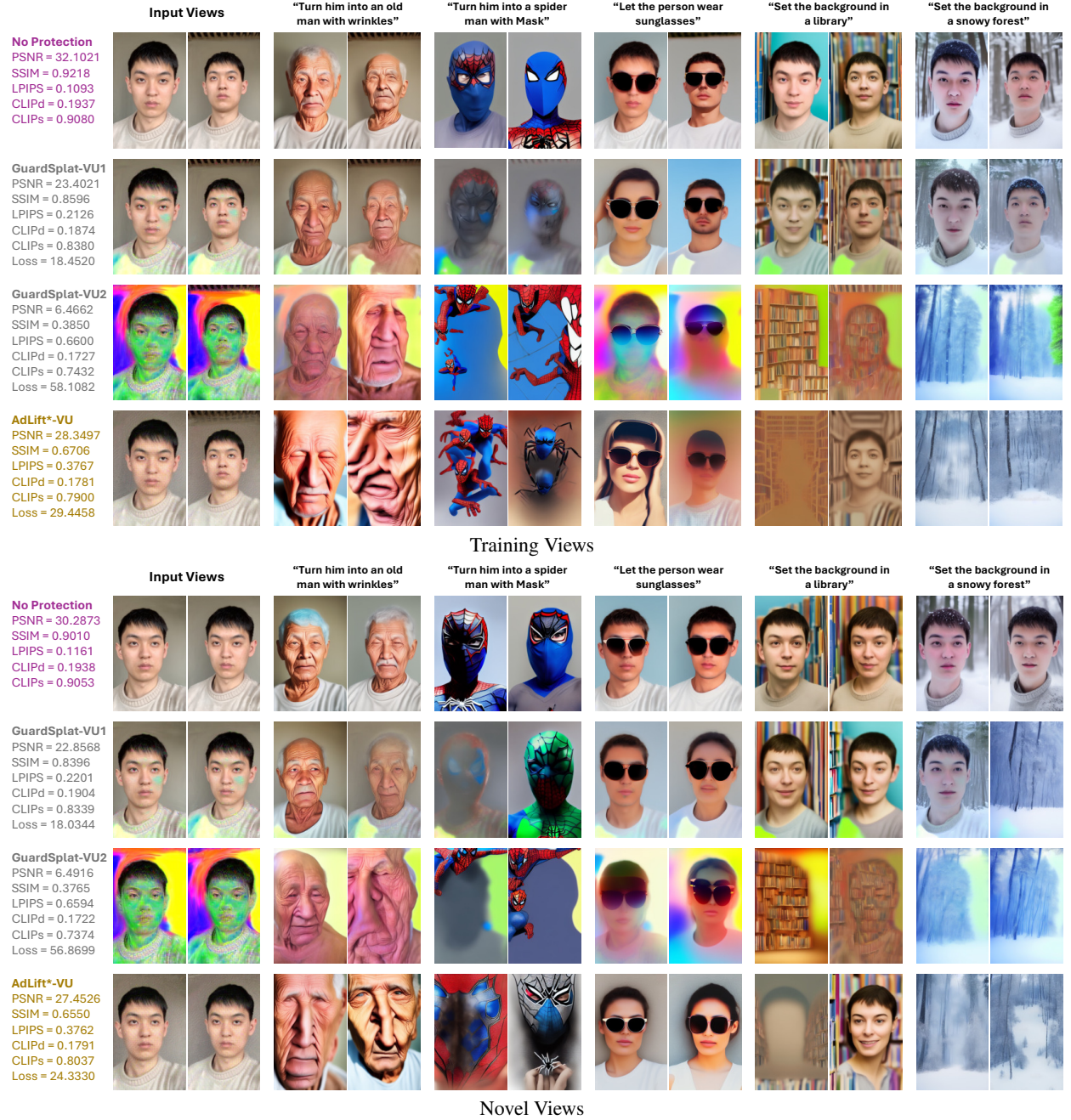


Figure 29: Comparison of qualitative editing results for GuardSplat-VU (with 2 different configurations) and AdLift*-VU at the same PSNR-level or anti-editing-level (Fangzhou).

replace original watermark decoding loss with our adversarial objective so that all methods are optimized toward the same protection goal.

The quantitative results are provided in Table 8 (training views) and Table 9 (novel views). We report protection performance under similar perceptual quality (similar PSNR). We also include representative qualitative comparisons in Figure 30 (training views) and Figure 31 (novel views). From the results, AdLift consistently achieves stronger anti-editing performance under similar invisibility constraints.

Table 8: Comparison with more baselines at the similar PSNR-level (training views). Bracketed values indicate changes relative to the unprotected baseline. Best results are highlighted in **bold**.

Method	SSIM (\uparrow)	PSNR (\uparrow)	LPIPS (\downarrow)	CLIP _d (\downarrow)	CLIP _s (\downarrow)	FID (\uparrow)	F _{1/8} (\downarrow)	F ₈ (\downarrow)
Face								
No Protection	0.9381	32.6436	0.0668	0.1685	0.8852	22.0270	0.9958	0.9947
GuardSplat-(SH)-VU	0.9348	31.7765	0.0802	0.1649 (-0.0036)	0.8769 (-0.0083)	26.2044 (+4.1774)	0.9952 (-0.0006)	0.9949 (0.0002)
GuardSplat-(SH)-VT	0.9319	28.8520	0.0930	0.1630 (-0.0055)	0.8643 (-0.0209)	28.4026 (+6.3756)	0.9923 (-0.0035)	0.9919 (-0.0028)
GuardSplat-(PC)-VU	0.8143	25.2876	0.1557	0.1605 (-0.0080)	0.8592 (-0.0260)	32.1277 (+10.1007)	0.9873 (-0.0085)	0.9910 (-0.0037)
GuardSplat-(PC)-VT	0.7979	24.4582	0.1779	0.1583 (-0.0102)	0.8456 (-0.0396)	37.3899 (+15.3629)	0.9813 (-0.0145)	0.9822 (-0.0125)
GuardSplat-(Full)-VU	0.8113	25.1306	0.1580	0.1617 (-0.0068)	0.8581 (-0.0271)	32.5037 (+10.4767)	0.9838 (-0.0120)	0.9887 (-0.0060)
GuardSplat-(Full)-VT	0.8016	24.6235	0.1775	0.1581 (-0.0104)	0.8493 (-0.0359)	36.9855 (+14.9585)	0.9816 (-0.0142)	0.9818 (-0.0129)
GaussianMarker-VU	0.9351	28.8343	0.0802	0.1596 (-0.0089)	0.8590 (-0.0262)	32.4431 (+10.4161)	0.9845 (-0.0113)	0.9916 (-0.0031)
GaussianMarker-VT	0.9364	28.8833	0.0720	0.1620 (-0.0065)	0.8665 (-0.0187)	26.3699 (+4.3429)	0.9929 (-0.0029)	0.9942 (-0.0005)
AdLift*-VU	0.7001	28.3963	0.3774	0.1554 (-0.0131)	0.7620 (-0.1232)	88.5865 (+66.5595)	0.8954 (-0.1004)	0.8742 (-0.1205)
Fangzhou								
No Protection	0.9218	32.1021	0.1093	0.1937	0.9080	23.7996	0.9817	0.9795
GuardSplat-(SH)-VU	0.8682	24.3325	0.1952	0.1882 (-0.0055)	0.8482 (-0.0598)	49.5017 (+25.7021)	0.9419 (-0.0398)	0.9716 (-0.0079)
GuardSplat-(SH)-VT	0.8727	24.2598	0.2198	0.1871 (-0.0066)	0.8588 (-0.0492)	43.0895 (+19.2899)	0.9325 (-0.0492)	0.9375 (-0.0420)
GuardSplat-(PC)-VU	0.8734	26.4272	0.1810	0.1863 (-0.0074)	0.8811 (-0.0269)	32.6075 (+8.8079)	0.9646 (-0.0171)	0.9669 (-0.0126)
GuardSplat-(PC)-VT	0.8683	27.0370	0.1756	0.1866 (-0.0071)	0.8804 (-0.0276)	35.9910 (+12.1914)	0.9138 (-0.0679)	0.9229 (-0.0566)
GuardSplat-(Full)-VU	0.8712	27.5267	0.1743	0.1906 (-0.0031)	0.8896 (-0.0184)	32.9438 (+9.1442)	0.9501 (-0.0316)	0.9547 (-0.0248)
GuardSplat-(Full)-VT	0.8590	27.0691	0.1821	0.1876 (-0.0061)	0.8778 (-0.0302)	36.4141 (+12.6145)	0.9598 (-0.0219)	0.9473 (-0.0322)
GaussianMarker-VU	0.9200	28.0355	0.1455	0.1907 (-0.0030)	0.8858 (-0.0222)	34.3784 (+10.5788)	0.9695 (-0.0122)	0.9672 (-0.0123)
GaussianMarker-VT	0.8637	23.7295	0.2460	0.1865 (-0.0072)	0.8296 (-0.0784)	57.1012 (+33.3016)	0.9015 (-0.0802)	0.9368 (-0.0427)
AdLift*-VU	0.6706	28.3497	0.3767	0.1781 (-0.0156)	0.7900 (-0.1180)	84.2180 (+60.4184)	0.8030 (-0.1787)	0.7749 (-0.2046)

Table 9: Comparison with more baselines at the similar PSNR-level (novel views). Bracketed values indicate changes relative to the unprotected baseline. Best results are highlighted in **bold**.

Method	SSIM (\uparrow)	PSNR (\uparrow)	LPIPS (\downarrow)	CLIP _d (\downarrow)	CLIP _s (\downarrow)	FID (\uparrow)	F _{1/8} (\downarrow)	F ₈ (\downarrow)
Face								
No Protection	0.8590	26.0390	0.1292	0.1704	0.8730	76.2210	0.9882	0.9835
GuardSplat-(SH)-VU	0.8552	25.7744	0.1442	0.1654 (-0.0050)	0.8666 (-0.0064)	83.8178 (+7.5968)	0.9834 (-0.0048)	0.9843 (0.0008)
GuardSplat-(SH)-VT	0.8528	25.0700	0.1571	0.1623 (-0.0081)	0.8550 (-0.0180)	80.3380 (+4.1170)	0.9901 (0.0019)	0.9879 (0.0044)
GuardSplat-(PC)-VU	0.7852	23.8763	0.1799	0.1667 (-0.0037)	0.8575 (-0.0155)	85.5826 (+9.3616)	0.9789 (-0.0093)	0.9790 (-0.0045)
GuardSplat-(PC)-VT	0.7712	23.2702	0.2004	0.1652 (-0.0052)	0.8480 (-0.0250)	91.1785 (+14.9575)	0.9752 (-0.0130)	0.9783 (-0.0052)
GuardSplat-(Full)-VU	0.7819	23.7877	0.1826	0.1658 (-0.0046)	0.8535 (-0.0195)	87.5892 (+11.3682)	0.9801 (-0.0081)	0.9762 (-0.0073)
GuardSplat-(Full)-VT	0.7752	23.4051	0.1983	0.1622 (-0.0082)	0.8505 (-0.0225)	90.4853 (+14.2643)	0.9748 (-0.0134)	0.9774 (-0.0061)
GaussianMarker-VU	0.8566	24.4911	0.1404	0.1628 (-0.0076)	0.8578 (-0.0152)	81.2042 (+4.9832)	0.9772 (-0.0110)	0.9770 (-0.0065)
GaussianMarker-VT	0.8567	24.8557	0.1346	0.1647 (-0.0057)	0.8608 (-0.0122)	81.1457 (+4.9247)	0.9849 (-0.0033)	0.9798 (-0.0037)
AdLift*-VU	0.6367	25.6115	0.4018	0.1586 (-0.0118)	0.7786 (-0.0944)	129.8172 (+53.5962)	0.8807 (-0.1075)	0.9279 (-0.0556)
Fangzhou								
No Protection	0.9010	30.2873	0.1161	0.1938	0.9053	51.7357	0.9905	0.9913
GuardSplat-(SH)-VU	0.8484	23.7358	0.2038	0.1905 (-0.0033)	0.8464 (-0.0589)	80.7992 (+29.0635)	0.9493 (-0.0412)	0.9679 (-0.0234)
GuardSplat-(SH)-VT	0.8546	23.6860	0.2254	0.1876 (-0.0062)	0.8570 (-0.0483)	71.4061 (+19.6704)	0.9533 (-0.0372)	0.9449 (-0.0464)
GuardSplat-(PC)-VU	0.8608	25.7609	0.1861	0.1880 (-0.0058)	0.8763 (-0.0290)	62.2475 (+10.5118)	0.9573 (-0.0332)	0.9629 (-0.0284)
GuardSplat-(PC)-VT	0.8570	26.3485	0.1807	0.1900 (-0.0038)	0.8807 (-0.0246)	65.9022 (+14.1665)	0.9403 (-0.0502)	0.9583 (-0.0330)
GuardSplat-(Full)-VU	0.8582	26.7445	0.1795	0.1903 (-0.0035)	0.8824 (-0.0229)	62.6535 (+10.9178)	0.9541 (-0.0364)	0.9543 (-0.0370)
GuardSplat-(Full)-VT	0.8480	26.3622	0.1866	0.1898 (-0.0040)	0.8752 (-0.0301)	67.569 (+15.8333)	0.9296 (-0.0609)	0.9403 (-0.0510)
GaussianMarker-VU	0.8998	26.8220	0.1516	0.1914 (-0.0024)	0.8844 (-0.0209)	64.0244 (+12.2887)	0.9735 (-0.0170)	0.9726 (-0.0187)
GaussianMarker-VT	0.8510	23.2438	0.2488	0.1872 (-0.0066)	0.8265 (-0.0788)	87.4162 (+35.6805)	0.8793 (-0.1112)	0.9319 (-0.0594)
AdLift*-VU	0.6550	27.4526	0.3762	0.1791 (-0.0147)	0.8037 (-0.1016)	102.6782 (+50.9425)	0.8337 (-0.1568)	0.8794 (-0.1119)

F.2 Transferability of AdLift

We additionally evaluate whether AdLift, which aims at lifting 2D adversarial perturbations into the 3D Gaussian space, can inherit the transferability in 2D adversarial protection.



Figure 30: Comparison of qualitative editing results between additional baselines and AdLift*-VU (training views).



Figure 31: Comparison of qualitative editing results between additional baselines and AdLift*-VU (novel views).

Table 10: Transferability of AdLift (training views). Bracketed values indicate changes relative to the unprotected baseline. Best results are highlighted in **bold**.

Edit Pipelines	Method	CLIP _d (↓)	CLIP _s (↓)	FID (↑)	F _{1/8} (↓)	F ₈ (↓)
Face						
IP2P	No Protection	0.1685	0.8852	22.0270	0.9958	0.9947
	AdLift*-VU	0.1554 (-0.0131)	0.7620 (-0.1232)	88.5865 (+66.5595)	0.8954 (-0.1004)	0.8742 (-0.1205)
	AdLift*-VT	0.1561 (-0.0124)	0.8272 (-0.0580)	45.1351 (+23.1081)	0.9545 (-0.0413)	0.9650 (-0.0297)
MagicBrush	No Protection	0.1741	0.8776	22.1594	0.9926	0.9885
	AdLift*-VU	0.1420 (-0.0321)	0.7457 (-0.1319)	69.4154 (+47.2560)	0.9305 (-0.0621)	0.9297 (-0.0588)
	AdLift*-VT	0.1588 (-0.0153)	0.8138 (-0.0638)	48.8487 (+26.6893)	0.9642 (-0.0284)	0.9540 (-0.0345)
SDEdit	No Protection	0.1659	0.7811	25.2357	0.9913	0.9894
	AdLift*-VU	0.1448 (-0.0211)	0.7141 (-0.067)	58.5985 (+33.3628)	0.8436 (-0.1477)	0.9484 (-0.0410)
	AdLift*-VT	0.1633 (-0.0026)	0.7131 (-0.068)	62.6101 (+37.3744)	0.8372 (-0.1541)	0.9532 (-0.0362)
SDXL-IP2P	No Protection	0.1053	0.7124	26.7935	0.9908	0.9899
	AdLift*-VU	0.1031 (-0.0022)	0.6509 (-0.0615)	48.6225 (+21.8290)	0.9691 (-0.0217)	0.9540 (-0.0359)
	AdLift*-VT	0.1016 (-0.0037)	0.6681 (-0.0443)	44.9257 (+18.1322)	0.9771 (-0.0137)	0.9512 (-0.0387)
Fangzhou						
IP2P	No Protection	0.1937	0.9080	23.7996	0.9817	0.9795
	AdLift*-VU	0.1781 (-0.0156)	0.7900 (-0.1180)	84.2180 (+60.4184)	0.8030 (-0.1787)	0.7749 (-0.2046)
	AdLift*-VT	0.1776 (-0.0161)	0.8198 (-0.0882)	56.5018 (+32.7022)	0.8721 (-0.1096)	0.8839 (-0.0956)
MagicBrush	No Protection	0.1839	0.8583	40.1794	0.8484	0.7938
	AdLift*-VU	0.1625 (-0.0214)	0.7548 (-0.1035)	105.8215 (+65.6421)	0.7135 (-0.1349)	0.5795 (-0.2143)
	AdLift*-VT	0.1611 (-0.0228)	0.8021 (-0.0562)	89.8512 (+49.6718)	0.5955 (-0.2529)	0.5720 (-0.2218)
SDEdit	No Protection	0.1224	0.7587	19.3086	0.9785	0.9795
	AdLift*-VU	0.1213 (-0.0011)	0.7148 (-0.0439)	88.8757 (+69.5671)	0.6992 (-0.2793)	0.8442 (-0.1353)
	AdLift*-VT	0.1179 (-0.0045)	0.6794 (-0.0793)	109.4655 (+90.1569)	0.5921 (-0.3864)	0.7453 (-0.2342)
SDXL-IP2P	No Protection	0.0777	0.7533	29.4324	0.9422	0.9106
	AdLift*-VU	0.0719 (-0.0058)	0.7322 (-0.0211)	47.7706 (+18.3382)	0.9354 (-0.0068)	0.8700 (-0.0406)
	AdLift*-VT	0.0738 (-0.0039)	0.7338 (-0.0195)	44.6247 (+15.1923)	0.9273 (-0.0149)	0.8019 (-0.1087)

Experimental setup: We train AdLift using SDv1.5-IP2P [11] as the surrogate editing model (the same as our paper), and then test it against three unseen editing models, including different editing pipelines and fine-tuned variants:

- MagicBrush [69]: Enhanced fine-tuned version of SDv1.5-IP2P on MagicBrush.
- SDEdit [70]: A diffusion-based editing framework that generates edited images by noising and denoising an input image, without requiring instruction-conditioned fine-tuning.
- SDXL-IP2P [11, 71]: Instruction fine-tuning of Stable Diffusion XL (SDXL).

The quantitative results of transferability are reported in Table 10 (training views) and Table 11 (novel views). Qualitative results are shown in Figure 32. Empirically, across all unseen editing models, AdLift can degrade editing qualities compared to the unprotected 3DGS asset, demonstrating that the protective effect generalizes beyond the surrogate model. This suggests that the proposed AdLift preserves the transferability behavior of 2D adversarial perturbations, even after being lifted into the 3D Gaussian domain.

F.3 Robustness to Purification

To evaluate robustness under purification, we follow the evaluation protocol used in prior 2D anti-editing works [21, 22] to test our method against two purification strategies, including a diffusion-based purification method (DiffPure [72]) and a standard compression method (JPEG compression [73]). The quantitative results are reported in Table 12 (training views) and Table 13 (novel views). Qualitative results are shown in Figure 33.

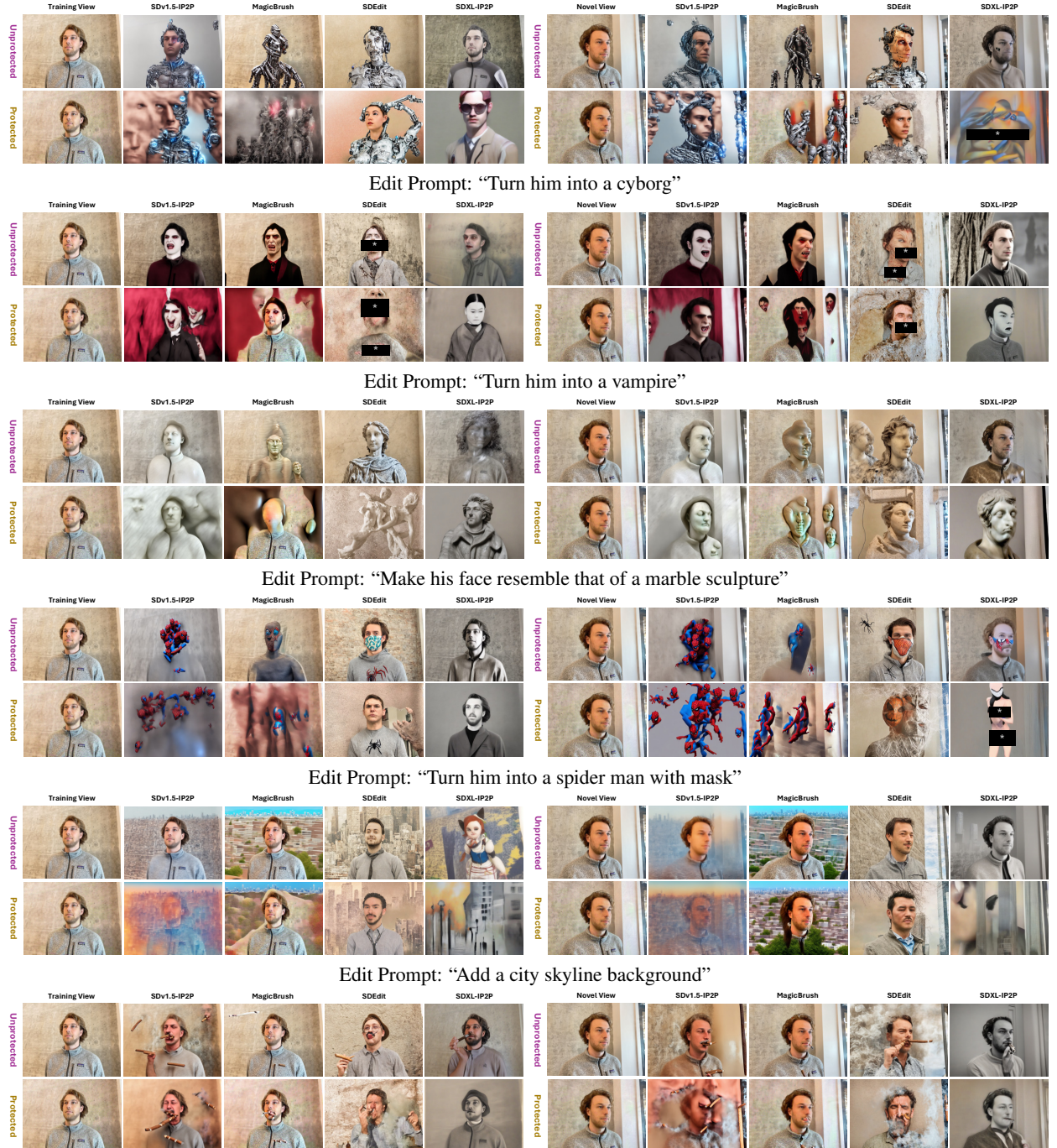
Our findings show that AdLift exhibit similar behavior to 2D adversarial protection: they remain effective under JPEG compression-based purification and generalize across unseen views. While diffusion-based purification reduces protection strength, AdLift still outperforms unprotected 3DGS assets.

Table 11: Transferability of AdLift (novel views). Bracketed values indicate changes relative to the unprotected baseline. Best results are highlighted in **bold**.

Edit Pipelines	Method	CLIP _d (↓)	CLIP _s (↓)	FID (↑)	F _{1/8} (↓)	F ₈ (↓)
Face						
IP2P	No Protection	0.1704	0.8730	76.2210	0.9882	0.9835
	AdLift*-VU	0.1586 (-0.0118)	0.7786 (-0.0944)	129.8172 (+53.5962)	0.8807 (-0.1075)	0.9279 (-0.0556)
	AdLift*-VT	0.1595 (-0.0109)	0.8285 (-0.0445)	93.4765 (+17.2555)	0.9473 (-0.0409)	0.9694 (-0.0141)
MagicBrush	No Protection	0.1769	0.8635	78.1133	0.9784	0.9638
	AdLift*-VU	0.1475 (-0.0294)	0.7659 (-0.0976)	120.0269 (+41.9136)	0.9150 (-0.0634)	0.9145 (-0.0493)
	AdLift*-VT	0.1607 (-0.0162)	0.8148 (-0.0487)	100.0880 (+21.9747)	0.9657 (-0.0127)	0.9570 (-0.0068)
SDEdit	No Protection	0.1708	0.7727	89.2094	0.9568	0.9722
	AdLift*-VU	0.1554 (-0.0154)	0.7397 (-0.033)	104.9600 (+15.7506)	0.9618 (0.0050)	0.9575 (-0.0147)
	AdLift*-VT	0.1751 (0.0043)	0.7353 (-0.0374)	118.0674 (+28.8580)	0.8806 (-0.0762)	0.9443 (-0.0279)
SDXL-IP2P	No Protection	0.1140	0.7012	93.6249	0.9707	0.9672
	AdLift*-VU	0.1094 (-0.0046)	0.6481 (-0.0531)	115.9670 (+22.3421)	0.9214 (-0.0493)	0.9289 (-0.0383)
	AdLift*-VT	0.1081 (-0.0059)	0.6693 (-0.0319)	112.9657 (+19.3408)	0.9383 (-0.0324)	0.9274 (-0.0398)
Fangzhou						
IP2P	No Protection	0.1938	0.9053	51.7357	0.9905	0.9913
	AdLift*-VU	0.1791 (-0.0147)	0.8037 (-0.1016)	102.6782 (+50.9425)	0.8337 (-0.1568)	0.8794 (-0.1119)
	AdLift*-VT	0.1788 (-0.0150)	0.8148 (-0.0905)	86.0002 (+34.2645)	0.8862 (-0.1043)	0.8676 (-0.1237)
MagicBrush	No Protection	0.1812	0.8566	73.9738	0.9032	0.8124
	AdLift*-VU	0.1605 (-0.0207)	0.7608 (-0.0958)	144.9615 (+70.9877)	0.7101 (-0.1931)	0.6113 (-0.2011)
	AdLift*-VT	0.1581 (-0.0231)	0.7998 (-0.0568)	124.9021 (+50.9283)	0.6838 (-0.2194)	0.5643 (-0.2481)
SDEdit	No Protection	0.1220	0.7578	68.4325	0.9802	0.9621
	AdLift*-VU	0.1292 (0.0072)	0.7300 (-0.0278)	124.4493 (+56.0168)	0.8783 (-0.1019)	0.9191 (-0.0430)
	AdLift*-VT	0.1194 (-0.0026)	0.6755 (-0.0823)	165.0488 (+96.6163)	0.6478 (-0.3324)	0.6729 (-0.2892)
SDXL-IP2P	No Protection	0.0738	0.7496	75.9508	0.9628	0.9113
	AdLift*-VU	0.0695 (-0.0043)	0.7321 (-0.0175)	100.9508 (+25.0000)	0.9127 (-0.0501)	0.9112 (-0.0001)
	AdLift*-VT	0.0715 (-0.0023)	0.7331 (-0.0165)	93.3964 (+17.4456)	0.9346 (-0.0282)	0.8424 (-0.0689)

Table 12: Robustness of AdLift against purification methods (training views). Bracketed values indicate changes relative to the unprotected baseline.

Method	CLIP _d (↓)	CLIP _s (↓)	FID (↑)	F _{1/8} (↓)	F ₈ (↓)
Face					
No Protection	0.1685	0.8852	22.0270	0.9958	0.9947
AdLift*-VU	0.1554 (-0.0131)	0.7620 (-0.1232)	88.5865 (+66.5595)	0.8954 (-0.1004)	0.8742 (-0.1205)
AdLift*-VU-JPEG	0.1548 (-0.0137)	0.7851 (-0.1001)	69.2879 (+47.2609)	0.9375 (-0.0583)	0.9359 (-0.0588)
AdLift*-VU-Difppure	0.1549 (-0.0136)	0.8173 (-0.0679)	51.5645 (+29.5375)	0.9753 (-0.0205)	0.9727 (-0.0220)
Fangzhou					
No Protection	0.1937	0.9080	23.7996	0.9817	0.9795
AdLift*-VU	0.1781 (-0.0156)	0.7900 (-0.1180)	84.2180 (+60.4184)	0.8030 (-0.1787)	0.7749 (-0.2046)
AdLift*-VU-JPEG	0.1791 (-0.0146)	0.8218 (-0.0862)	61.7341 (+37.9345)	0.9197 (-0.0620)	0.9332 (-0.0463)
AdLift*-VU-Difppure	0.1860 (-0.0077)	0.8640 (-0.0440)	35.8747 (+12.0751)	0.9777 (-0.0040)	0.9670 (-0.0125)



Edit Prompt: "Let the person smoke a cigar"

Figure 32: Transferability of AdLift. **Warning:** Following safety and ethical guidelines, harmful or sensitive content (e.g., sexual imagery, or violence) is masked in the figures.

Table 13: Robustness of AdLift against purification methods (novel views). Bracketed values indicate changes relative to the unprotected baseline.

Method	CLIP _d (↓)	CLIP _s (↓)	FID (↑)	F _{1/8} (↓)	F ₈ (↓)
Face					
No Protection	0.1704	0.8730	76.2210	0.9882	0.9835
AdLift*-VU	0.1586 (-0.0118)	0.7786 (-0.0944)	129.8172 (+53.5962)	0.8807 (-0.1075)	0.9279 (-0.0556)
AdLift*-VU-JPEG	0.1573 (-0.0131)	0.7947 (-0.0783)	116.7051 (+40.4841)	0.9420 (-0.0462)	0.9486 (-0.0349)
AdLift*-VU-Diffpure	0.1573 (-0.0131)	0.8162 (-0.0568)	107.5986 (+31.3776)	0.9639 (-0.0243)	0.9432 (-0.0403)
Fangzhou					
No Protection	0.1938	0.9053	51.7357	0.9905	0.9913
AdLift*-VU	0.1791 (-0.0147)	0.8037 (-0.1016)	102.6782 (+50.9425)	0.8337 (-0.1568)	0.8794 (-0.1119)
AdLift*-VU-JPEG	0.1822 (-0.0116)	0.8229 (-0.0824)	85.8403 (+34.1046)	0.9353 (-0.0552)	0.9519 (-0.0394)
AdLift*-VU-Diffpure	0.1883 (-0.0055)	0.8618 (-0.0435)	64.7646 (+13.0289)	0.9756 (-0.0149)	0.9687 (-0.0226)



Figure 33: Robustness of AdLift against purification.

E.4 Generality of AdLift

To show the generality of AdLift, we extend our evaluation by including two additional 360-degree scenes. The corresponding quantitative results are reported in Table 14 (training views) and Table 15 (novel views). Besides, qualitative results are shown in Figure 34. Across all metrics and scenes, our method consistently outperforms both unprotected 3DGS assets and baseline methods in terms of anti-editing effectiveness.

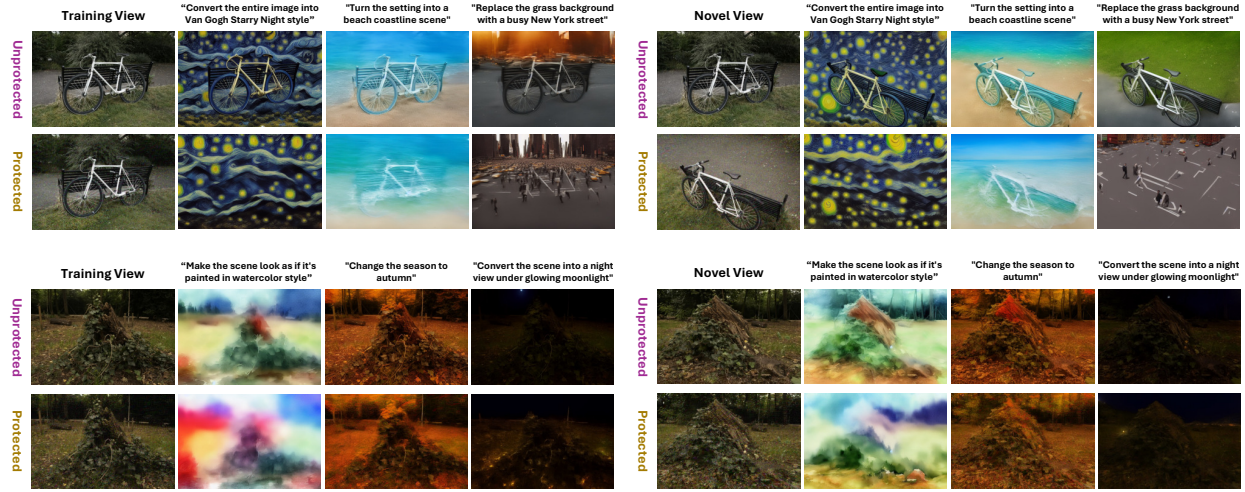


Figure 34: Qualitative results of AdLift on more scenes.

Table 14: Performance of AdLift on more scenes (training views). Bracketed values indicate changes relative to the unprotected baseline. Best results are highlighted in **bold**.

Method	SSIM (\uparrow)	PSNR (\uparrow)	LPIPS (\downarrow)	CLIP _d (\downarrow)	CLIP _s (\downarrow)	FID (\uparrow)	F _{1/8} (\downarrow)	F ₈ (\downarrow)
Bicycle								
No Protection	0.9132	27.5901	0.0536	0.1935	0.8995	17.1704	0.9947	0.9944
Fit2D-VU	0.8084	25.5982	0.1818	0.1914 (-0.0021)	0.8714 (-0.0281)	25.6811 (+8.5107)	0.9740 (-0.0207)	0.9860 (-0.0084)
Fit2D-VT	0.8186	25.8145	0.1126	0.1889 (-0.0046)	0.8805 (-0.0190)	23.3785 (+6.2081)	0.9863 (-0.0084)	0.9885 (-0.0059)
AdLift*-VU	0.7822	25.8218	0.2388	0.1851 (-0.0084)	0.8250 (-0.0745)	48.7802 (+31.6098)	0.9218 (-0.0729)	0.9600 (-0.0344)
AdLift*-VT	0.7899	26.0401	0.1259	0.1837 (-0.0098)	0.8589 (-0.0406)	30.5979 (+13.4275)	0.9714 (-0.0233)	0.9825 (-0.0119)
Stump								
No Protection	0.9456	32.2618	0.0353	0.1689	0.9298	26.0890	0.9954	0.9964
Fit2D-VU	0.7976	27.2747	0.2089	0.1651 (-0.0038)	0.8846 (-0.0452)	47.1604 (+21.0714)	0.9716 (-0.0238)	0.9739 (-0.0225)
Fit2D-VT	0.8145	28.0254	0.1172	0.1676 (-0.0013)	0.8953 (-0.0345)	42.4515 (+16.3625)	0.9493 (-0.0461)	0.9666 (-0.0298)
AdLift*-VU	0.7838	27.4652	0.2616	0.1657 (-0.0032)	0.8491 (-0.0807)	66.9380 (+40.8490)	0.8910 (-0.1044)	0.9021 (-0.0943)
AdLift*-VT	0.8001	28.2688	0.1358	0.1669 (-0.0020)	0.8739 (-0.0559)	59.8454 (+33.7564)	0.8851 (-0.1103)	0.8864 (-0.1100)

Table 15: Performance of AdLift on more scenes (novel views). Bracketed values indicate changes relative to the unprotected baseline. Best results are highlighted in **bold**.

Method	SSIM (\uparrow)	PSNR (\uparrow)	LPIPS (\downarrow)	CLIP _d (\downarrow)	CLIP _s (\downarrow)	FID (\uparrow)	F _{1/8} (\downarrow)	F ₈ (\downarrow)
Bicycle								
No Protection	0.8431	26.743	0.0672	0.1914	0.9019	53.7759	0.9826	0.9840
Fit2D-VU	0.7306	24.9763	0.2004	0.1897 (-0.0017)	0.1874 (-0.7145)	61.5747 (+7.7988)	0.9659 (-0.0167)	0.9725 (-0.0115)
Fit2D-VT	0.7446	25.3495	0.1297	0.1848 (-0.0066)	0.8839 (-0.0180)	61.2288 (+7.4529)	0.9671 (-0.0155)	0.9743 (-0.0097)
AdLift*-VU	0.7019	24.4851	0.2650	0.1844 (-0.0070)	0.8384 (-0.0635)	91.9488 (+38.1729)	0.8726 (-0.1100)	0.9275 (-0.0565)
AdLift*-VT	0.7152	24.7930	0.1533	0.1798 (-0.0116)	0.8583 (-0.0436)	76.4528 (+22.6769)	0.9367 (-0.0459)	0.9564 (-0.0276)
Stump								
No Protection	0.8157	27.2135	0.0713	0.1652	0.9223	82.9066	0.9826	0.9852
Fit2D-VU	0.6754	24.5672	0.2095	0.1593 (-0.0059)	0.8933 (-0.0290)	103.8607 (+20.9541)	0.9702 (-0.0124)	0.9545 (-0.0307)
Fit2D-VT	0.6971	25.1350	0.1403	0.1607 (-0.0045)	0.9042 (-0.0181)	95.7885 (+12.8819)	0.9584 (-0.0242)	0.9732 (-0.0120)
AdLift*-VU	0.6607	24.3507	0.2498	0.1602 (-0.0050)	0.8685 (-0.0538)	114.4635 (+31.5569)	0.9023 (-0.0803)	0.9174 (-0.0678)
AdLift*-VT	0.6884	25.0868	0.1599	0.1602 (-0.0050)	0.8882 (-0.0341)	104.7286 (+21.8220)	0.8873 (-0.0953)	0.9181 (-0.0671)

G More Discussion and Limitation

G.1 Discussion

Differ from related works. Although related prior directions exist, they differ in goals and applicability:

- 3DGS watermarking (e.g., [15, 16])
 - Problem scope: 3DGS watermarking only provides passive traceability rather than actively resisting instruction-driven editing.
 - Methodology: Existing 3DGS watermarking approaches, which inject perturbations into Gaussian parameters relying on soft invisibility regularization over all (or selected) attributes, fail to balance between invisibility and adversarial effectiveness when applied to learning imperceptible adversarial perturbations against editing models. Our results in Tables 6 to 9 and Figures 3, 10, 11, 28 and 29 offers evidence supporting this point.
- 2D adversarial protection (e.g., [21, 22])
 - While conceptually aligned, these methods cannot be directly applied to 3DGS. As 3DGS representations use 3D Gaussian primitives instead of pixel-space representations.

Taken together, prior directions inform but do not solve our problem setting, which requires adversarially optimized, perceptually bounded, and view-consistent protection for 3DGS under instruction-driven editing pipelines.

Challenge of enabling anti-editing protection in 3DGS. We aim at addressing the practical challenge of enabling anti-editing protection in 3D Gaussian Splatting, where perturbations must remain view-consistent, perceptually bounded at rendering, and robust across 3D-aware editing pipelines. More importantly, unlike 2D pixel-based images, 3DGS stores information in Gaussian primitives with heterogeneous attributes, making direct transfer from 2D methods non-trivial. This setting introduces several core challenges:

- **View inconsistency of 2D adversarial perturbations:** Applying 2D adversarial optimization (like [C1-C2]) followed by 3D reconstruction may induces cross-view conflicts, and the resulting 3DGS suffers from underfitting and exhibits poor generalization to novel views (Figures 2 and 9).
- **Soft constraint limitations:** Although prior 3DGS watermarking methods introduce imperceptible perturbations using soft regularization on Gaussian parameters, directly applying 2D anti-editing objectives through such mechanisms fails to achieve a proper balance between invisibility and adversarial effectiveness (Tables 6 to 9 and Figures 3, 10, 11, 28 and 29).
- **No unified perturbation space:** 3DGS parameters consist of heterogeneous attributes (position, scale, opacity, SH coefficients), making it non-trivial to impose a unified perturbation budget analogous to PGD in 2D pixel space.

G.2 Limitations

Balance invisibility against protection effectiveness. Although AdLift show some balance, as AdLift consistently achieves stronger editing resistance while maintaining similar or better perceptual quality compared to a broader baselines. This also indicates that the learned perturbations are not trivial noise. In addition, further reducing perceptual impact while retaining protection strength is still an important direction.

Computation overhead. Lifting PGD into the 3DGS space introduces additional computational overhead. The increased cost is mainly due to the need to back-propagate gradients through the editing model on multiple rendered views in order to achieve view-generalizable protection. The computation scales with both the editing model complexity and the number of supervised viewpoints. This reflects an inherent challenge of adversarial learning for 3DGS and highlights opportunities for future efficiency improvements, such as using lightweight surrogate editing models or adaptive view-sampling strategies.

Robustness to purification. Our findings in Appendix F.3 show that AdLift exhibit similar behavior to 2D adversarial protection: they remain effective under JPEG compression-based purification and generalize across unseen views. While diffusion-based purification reduces protection strength, AdLift still outperforms unprotected 3DGS assets. We consider improving purification robustness, potentially by lifting purification-resilient 2D adversarial strategies into the 3D domain, as an important direction for future work.

Theoretical analysis. The current work is primarily empirical. Providing formal convergence guarantees for adversarial optimization in the context of 3D Gaussian Splatting is non-trivial due to the heterogeneous parameterization and the complexity of the differentiable rendering process. We view this as an important open research direction rather than a solved component of the field.

H More Experimental Details

H.1 Evaluation Metrics

Invisibility. We assess the visual fidelity of rendered views against the ground truth using three standard metrics: Peak Signal-to-Noise Ratio (PSNR), Structural Similarity Index (SSIM) [62], and Learned Perceptual Image Patch Similarity (LPIPS) [63]. Specifically, higher SSIM and PSNR, and lower LPIPS indicate better fidelity to the original image.

Protection Capability. To measure protection effectiveness, we adopt two CLIP-based metrics: CLIP Text-Image Directional Similarity (denoted as CLIP_d) and CLIP Image Similarity (CLIP_s).

CLIP_d evaluates how well the edit aligns with the input text instruction [53, 12, 52, 26], and is computed as:

$$\text{CLIP}_d = \text{CosineSimilarity}(C_i(x^{\text{edit}}) - C_i(x), C_t(t^{\text{out}}) - C_t(t^{\text{in}})), \quad (11)$$

where C_i and C_t denote the image and text encoders of CLIP, respectively. For each edit instruction, we predefine the corresponding input description t^{in} and target description t^{out} (details in Appendix H.2).

CLIP_s measures the similarity between edits applied to original and protected assets, defined as:

$$\text{CLIP}_s = \text{CosineSimilarity}(C_i(x_{\text{prot}}^{\text{edit}}), C_i(x_{\text{raw}}^{\text{edit}})). \quad (12)$$

In our setting, lower CLIP_d or CLIP_s values indicate stronger protection, since edits on protected assets deviate from instruction-following or from the corresponding edits on unprotected assets.

H.2 Editing Instructions

Editing instructions are partially collected from prior 3DGS editing works [52, 53, 12, 52, 26] and further extended using GPT-5, followed by careful human review. Finally, 25 high-quality instructions are curated for each scene, as shown in Tables 16 to 18.

For both IP2P-based 2D and 3D editing, these instructions serve as the editing inputs. When computing CLIP_d , the corresponding source and target description are encoded into text embeddings within the CLIP space, which are then compared with image embeddings to evaluate semantic alignment, as shown in Equation (11).

Table 16: Editing instructions and source/target descriptions for two forwarding face scenes.

Source Description	Target Description	Editing Instruction
a photo of a face of a man	a photo of a face of a Joker with green hair	turn him into a Joker with green hair
a photo of a face of a man	a photo of a face of an old man with wrinkles	turn him into an old man with wrinkles
a photo of a face of a man	a photo of a werewolf	Turn him into a werewolf
a photo of a face of a man	a photo of a cyborg	Turn him into a cyborg
a photo of a face of a man	a photo of a marble sculpture	Make his face resemble that of a marble sculpture
a photo of a face of a man	a photo of a face of a vampire	Turn him into a vampire
a photo of a face of a man	a photo of a face of a spider man with Mask	Turn him into a spider man with Mask
a photo of a face of a man	a photo of a face of a man with a moustache	turn him a moustache
a photo of a face of a man	a photo of a man wearing a pair of glasses	give him a pair of glasses
a photo of a face of a man	a photo of a face of a man with red hair	give him red hair
a photo of a face of a man	a photo of a face of a man with pink hair	Turn the person's hair pink
a photo of a face of a man	a photo of a face of a man with a tattoo	Let the person have a tattoo
a photo of a face of a man	a photo of a face of a man with elf-like ears	Add elf-like ears
a photo of a face of a man	a photo of a man wearing sunglasses	Let the person wear sunglasses
a photo of a face of a man	a photo of a face of a man smoking a cigar	Let the person smoke a cigar
a photo of a face of a man	a photo of a face of a man wearing a tiara	Place a tiara on the top of the head
a photo of a face of a man	a photo of a face of a man with a beach background	Change the background to a beach
a photo of a face of a man	a photo of a face of a man in a library background	Set the background in a library
a photo of a face of a man	a photo of a face of a man with a city skyline background	Add a city skyline background
a photo of a face of a man	a photo of a face of a man in a desert background	Change the background to a desert
a photo of a face of a man	a photo of a face of a man under a starry night sky	Set the background as a night sky with stars
a photo of a face of a man	a photo of a face of a man in a snowy forest	Set the background in a snowy forest
a photo of a face of a man	a photo of a face of a man in an office background	Put the man in an office background
a photo of a face of a man	a photo of a face of a man with a mountain background	Set the background to a mountain landscape
a photo of a face of a man	a photo of a face of a man standing under the moonlight	Let the person stand under the moon

Table 17: Editing instructions and source/target descriptions for the bear scene.

Source Description	Target Description	Editing Instruction
a photo of a bear statue in the forest	a photo of a grizzly bear in the forest	turn the bear into a grizzly bear
a photo of a bear statue in the forest	a photo of a polar bear in the forest	turn the bear into a polar bear
a photo of a bear statue in the forest	a photo of a panda in the forest	turn the bear into a panda
a photo of a bear statue in the forest	a photo of a golden bear in the forest	turn the bear into a golden bear
a photo of a bear statue in the forest	a photo of a robot bear in the forest	turn the bear into a robot bear
a photo of a bear statue in the forest	a photo of a skeleton bear in the forest	turn the bear into a skeleton bear
a photo of a bear statue in the forest	a photo of a bronze bear statue in the forest	turn the bear into a bronze statue
a photo of a bear statue in the forest	a photo of a glass bear in the forest	turn the bear into a glass sculpture
a photo of a bear statue in the forest	a photo of a wooden bear in the forest	turn the bear into a wooden bear
a photo of a bear statue in the forest	a photo of a giraffe in the forest	turn the bear into a giraffe
a photo of a bear statue in the forest	a photo of a fox in the forest	turn the bear into a fox
a photo of a bear statue in the forest	a photo of a raccoon in the forest	turn the bear into a raccoon
a photo of a bear statue in the forest	a photo of a bear statue in the snow	make the forest snowy
a photo of a bear statue in the forest	a photo of a bear statue in the forest at night	make it a night scene
a photo of a bear statue in the forest	a photo of a bear in the forest in the rain	make it raining
a photo of a bear statue in the forest	a photo of a bear statue in the forest during a storm	make it a stormy weather
a photo of a bear statue in the forest	a photo of a bear statue in the forest with a rainbow	add a rainbow in the background
a photo of a bear statue in the forest	a photo of a bear underwater	make it underwater
a photo of a bear statue in the forest	a photo of a bear in the desert	place the bear in a desert
a photo of a bear statue in the forest	a photo of a bear statue with fireflies in the forest	add fireflies around the bear
a photo of a bear statue in the forest	a photo of a mossy bear statue in the forest	add vines growing on the bear
a photo of a bear statue in the forest	a photo of a bear statue wearing a crown in the forest	put a crown on the bear
a photo of a bear statue in the forest	a photo of a chocolate bear in the forest	turn the bear into a chocolate sculpture
a photo of a bear statue in the forest	a photo of a crystal bear in the forest	turn the bear into a bear made of crystal
a photo of a bear statue in the forest	a photo of a fiery bear in the forest	turn the bear into a bear made of fire

Table 18: Editing instructions and source/target descriptions for the stone-horse scene.

Source Description	Target Description	Editing Instruction
a photo of a stone horse statue in front of the museum	a photo of a grizzly bear in front of the museum	turn the stone horse into a grizzly bear
a photo of a stone horse statue in front of the museum	a photo of a giraffe in front of the museum	turn the stone horse into a giraffe
a photo of a stone horse statue in front of the museum	a photo of a red panda in front of the museum	turn the stone horse into a red panda
a photo of a stone horse statue in front of the museum	a photo of a robot horse in front of the museum	turn the stone horse into a robot horse
a photo of a stone horse statue in front of the museum	a photo of a polar bear in front of the museum	turn the stone horse into a polar bear
a photo of a stone horse statue in front of the museum	a photo of a golden horse in front of the museum	turn the stone horse into a golden horse
a photo of a stone horse statue in front of the museum	a photo of a red horse in front of the museum	turn the stone horse into a red horse
a photo of a stone horse statue in front of the museum	a photo of a horse under the water in front of the museum	make it under the water
a photo of a stone horse statue in front of the museum	a photo of a horse in the snow in front of the museum	make it snowy
a photo of a stone horse statue in front of the museum	a photo of a horse at night in front of the museum	make it at night
a photo of a stone horse statue in front of the museum	a photo of a horse in the storm in front of the museum	make it in the storm
a photo of a stone horse statue in front of the museum	a photo of a zebra in front of the museum	turn the stone horse into a zebra
a photo of a stone horse statue in front of the museum	a photo of a unicorn in front of the museum	turn the stone horse into a unicorn
a photo of a stone horse statue in front of the museum	a photo of a pegasus in front of the museum	turn the stone horse into a pegasus
a photo of a stone horse statue in front of the museum	a photo of a knight riding the horse in front of the museum	add a knight riding the horse
a photo of a stone horse statue in front of the museum	a photo of a mossy horse statue in front of the museum	cover the horse with moss
a photo of a stone horse statue in front of the museum	a photo of an ice horse in front of the museum	turn the horse into ice sculpture
a photo of a stone horse statue in front of the museum	a photo of a graffiti-covered horse statue in front of the museum	paint the horse statue with graffiti
a photo of a stone horse statue in front of the museum	a photo of a horse in the desert in front of the museum	place the horse in the desert
a photo of a stone horse statue in front of the museum	a photo of a horse skeleton in front of the museum	turn the horse into a skeleton
a photo of a stone horse statue in front of the museum	a photo of a horse statue decorated with fairy lights in front of the museum	add fairy lights on the horse
a photo of a stone horse statue in front of the museum	a photo of a crowned horse in front of the museum	put a crown on the horse
a photo of a stone horse statue in front of the museum	a photo of a winged horse in front of the museum	add wings to the horse
a photo of a stone horse statue in front of the museum	a photo of a horse statue surrounded by butterflies in front of the museum	add butterflies around the horse
a photo of a stone horse statue in front of the museum	a photo of a glass horse in front of the museum	make the horse transparent like glass